https://doi.org/10.5194/egusphere-2026-4859
Preprint. Discussion started: 20 August 2026

RDycore-sediment v1.0: A two-dimensional sediment transport model for Earth system modeling

Dongyu Feng[1], Zeli Tan[1], Donghui Xu[1], Jeffrey Johnson[2], and Gautam Bisht[1]

[1]Atmospheric, Climate, and Earth Sciences Division, Pacific Northwest National Laboratory, Richland, Washington, USA
[2]Cohere Consulting, LLC, Seattle, 98105, Washington, USA

Correspondence to: Dongyu Feng (dongyu.feng@pnnl.gov)

Abstract. Sediment transport links land-surface erosion, river and floodplain morphology, reservoir storage, water quality, and downstream material delivery. Yet scalable two-dimensional (2-D) sediment transport representation remains limited in large-scale Earth system modeling frameworks. We present RDycore-sediment v1.0, an extension of the River Dynamical Core version 1.0 (RDycore v1.0), which adds conservative multi-class suspended sediment transport and local water-bed sediment exchange to RDycore v1.0's finite volume shallow water formulation. The model routes class-specific suspended sediment mass according to RDycore simulated hydrodynamics and accounts for bed erosion, deposition, active-layer exchange, and substrate-layer bed storage. In this first version, bed sediment mass is updated diagnostically, but bed elevation remains fixed and sediment dynamics does not feed back onto flow dynamics. Additionally, we extended the hydrodynamics model within RDycore to include hydrostatic reconstruction of the flow variables. RDycore-sediment is evaluated with both ideal and realistic benchmark cases, including 1) two conventional passive transport benchmarks, 2) a dam break erosion and deposition comparison with TELEMAC/GAIA, 3) a three-class method of manufactured solutions case, and 4) a Hurricane Harvey Houston benchmark driven by runoff and soil erosion inputs. In idealized tests, RDycore-sediment preserves passive transport and lake-at-rest states, reproduces TELEMAC/GAIA erosion and deposition in the idealized dam break, and achieves first-order convergence. For the Hurricane Harvey case, RDycore-sediment and TELEMAC/GAIA simulate comparable event-scale timing and total bed mass changes. The Hurricane Harvey case also highlights the importance of including coastal backwater effects and the use of well-balanced hydrodynamics for sediment applications in complex urban watersheds, as small errors in velocity and shear stress can bias the calculation of bed erosion and deposition. RDycore-sediment provides a scalable foundation for 2-D sediment routing in river and floodplain systems and supports future coupling with Earth system models across the land-river-ocean continuum.

1 Introduction

Sediment transport connects processes from hillslopes to rivers, floodplains, reservoirs, deltas, and oceans. Across these scales, sediment erosion, transport, temporary storage, and remobilization regulate soil loss, water quality, reservoir capacity, channel morphology, aquatic habitat, and the delivery of carbon and nutrients to coastal waters (Berhe et al., 2018; Dethier et al., 2022;

https://doi.org/10.5194/egusphere-2026-4859
Preprint. Discussion started: 20 August 2026

Syvitski et al., 2005; Vörösmarty et al., 2003; Walling, 1983). Climate variability and human activities can modify different parts of this continuum. Intensified rainfall and land disturbance may increase sediment production, whereas soil conservation, reservoirs, and river engineering may reduce or redistribute downstream fluxes (Guan et al., 2022; Li et al., 2021; Wang et al., 2016). Recent studies further demonstrate that sediment dynamics depend not only on water discharge but also on sediment availability, particle size, floodplain and reservoir storage, and spatially heterogeneous hydrodynamics (Feng et al., 2025; Lamb et al., 2020; Sun et al., 2021; Wohl et al., 2015). Sediment modeling is therefore needed from local river and floodplain applications to watershed- and continental-scale sediment transport along the land-river-ocean continuum.

Despite its importance, sediment transport remains difficult to predict across spatial scales. Although individual processes have been investigated using mechanistic models, detailed evaluation remains largely limited to laboratory flumes, rainfall experiments, or small idealized basins (Heng et al., 2011; Jomaa et al., 2012; Kim et al., 2013). Extrapolation to watersheds and larger domains is hindered not only by heterogeneous sediment sources and poorly constrained erosion parameters, but also by the ability to resolve complex river-floodplain dynamics and spatially variable bed shear stress (Feng et al., 2025; Lamb et al., 2020; Wohl et al., 2015). Representing these processes over large domains requires high-resolution topography, two-dimensional hydrodynamics, and computational scalability, creating a persistent trade-off among physical detail, data requirements, and computational feasibility in existing sediment models.

Existing river sediment models span a broad range of scales and process complexity. Regional and global models generally achieve scalability through reduced-complexity representations. BQART and HydroTrend estimate sediment export from basin-scale relationships among discharge, relief, climate, lithology, and human influence, but do not explicitly resolve sediment transport within river channels and floodplains (Kettner & Syvitski, 2008; Syvitski & Milliman, 2007). WBMsed distributes the BQART approach spatially, but retains its empirical sediment generation formulation and has limited skill in reproducing extreme daily fluxes (Cohen et al., 2013). Network models such as D-CASCADE represent reach-scale connectivity, multiple grain sizes, and sediment budgets, while relying on one-dimensional river networks and empirical transport capacity equations (Tangi et al., 2022). MOSART-sediment connects hillslope erosion, wash load, bed material transport, and reservoir trapping within an Earth system model (ESM) (Li et al., 2022). However, its one-dimensional routing framework does not resolve spatially heterogeneous floodplain hydraulics or two-dimensional (2-D) bed shear stress, and channel-floodplain exchange and sediment routing within reservoirs are simplified.

At watershed scales, empirical and semi-empirical models offer lower-cost alternatives for practical applications. SWMM, for example, represents sediment buildup and washoff from urban surfaces and subsequent routing through drainage networks using calibrated relationships (Gorgoglione et al., 2019). The model is useful for estimating event-scale loads and evaluating stormwater management practices but is not designed to resolve 2-D floodplain transport or water-bed exchange controlled by shear stress. More mechanistic watershed models couple sediment mass conservation with hydrologic or shallow-water equations.

https://doi.org/10.5194/egusphere-2026-4859
Preprint. Discussion started: 20 August 2026

Hydraulic and morphodynamic modeling systems form another major branch of sediment modeling. Shallow-water-equation-based models can couple flow dynamics with suspended sediment transport, bedload transport, shear stress driven erosion, deposition, and bed evolution. Commonly used river and floodplain modeling systems include TELEMAC-MASCARET (Tassi et al., 2023; Villaret et al., 2013), HEC-RAS sediment modules (Brunner & Gibson, 2005), BASEMENT (Vanzo et al., 2021), iRIC (Shimizu et al., 2020), PIHM (Li & Duffy, 2011), and Delft3D (Lesser et al., 2004). These models provide different levels of support for multiple grain-size sediment classes, active-layer bed structure, and morphodynamic bed updating. Their greater physical details require fine-resolution topography, sediment boundary conditions, bed material properties, and substantial calibration and computational resources. Consequently, their applications are often limited to individual river reaches, urban floodplains, reservoirs, or estuaries rather than continental or ESM domains.

RDycore was developed to address the corresponding hydrodynamic scale gap in ESMs (i.e. E3SM (Golaz et al., 2019; Golaz et al., 2022)) (Bisht et al., 2025; Xu et al., 2026). It solves the 2-D shallow-water equations on structured or unstructured meshes and uses PETSc and libCEED for scalable execution on CPUs and GPUs (Balay et al., 2021; Brown et al., 2021). As RDycore develops into a higher-fidelity alternative to E3SM's river component MOSART (Li et al., 2013), RDycore-sediment can provide a corresponding alternative to MOSART-sediment for applications in which spatial hydrodynamics are important. The 2-D representation can explicitly resolve overland flow pathways, wetting and drying, channel–floodplain exchange, and spatial variations in velocity and bed shear stress at ultra-high resolutions (O(1m)) at large spatial scales. Thus, RDycore-sediment targets the corresponding scale gap: representing spatially resolved suspended sediment transport and local water-bed exchange in a framework suitable for large-domain ESM applications.

Coupling RDycore-sediment into E3SM would establish a land-river-ocean sediment transport continuum (Fig. 1). Upstream, the E3SM Land Model (ELM) can supply runoff and sediment generated by rainfall- and runoff-driven soil erosion (Tan et al., 2022; Tan et al., 2018), including particle-associated carbon, nitrogen, and phosphorus (Tan et al., 2021; Tan et al., 2020). RDycore-sediment can then route the ELM-simulated tracers through overland flow and river environments. At river mouths, water, sediment, and particulate biogeochemical fluxes could be transferred directly to the E3SM ocean model rather than prescribed from an external or climatological dataset. Furthermore, two-way river–ocean coupling would allow ocean water levels to influence upstream flow and sediment exchange during high tides and storm surge (Feng et al., 2024). Such coupling would improve mass consistency among model components and support investigation of lateral carbon and nutrient transport across the land–river–ocean continuum, which remains poorly constrained in current Earth system models (Liu et al., 2024; Regnier et al., 2022; Ward et al., 2020).

This paper presents RDycore-sediment v1.0. The model adds conservative transport of multiple suspended sediment classes and local water-bed exchange to RDycore's finite-volume shallow-water formulation. Bed erosion and deposition follow the Partheniades and GAIA formulations (Partheniades, 1965; Tassi et al., 2023). The current version tracks suspended and bed sediment mass but does not update bed elevation. Bedload, Exner-based morphodynamics, and morphology–flow feedback remain future developments. We document the governing equations and implementation and evaluate the model progressively

https://doi.org/10.5194/egusphere-2026-4859
Preprint. Discussion started: 20 August 2026

using passive-transport tests, erosion-deposition benchmarks, manufactured solutions, and a Hurricane Harvey comparison with TELEMAC/GAIA.

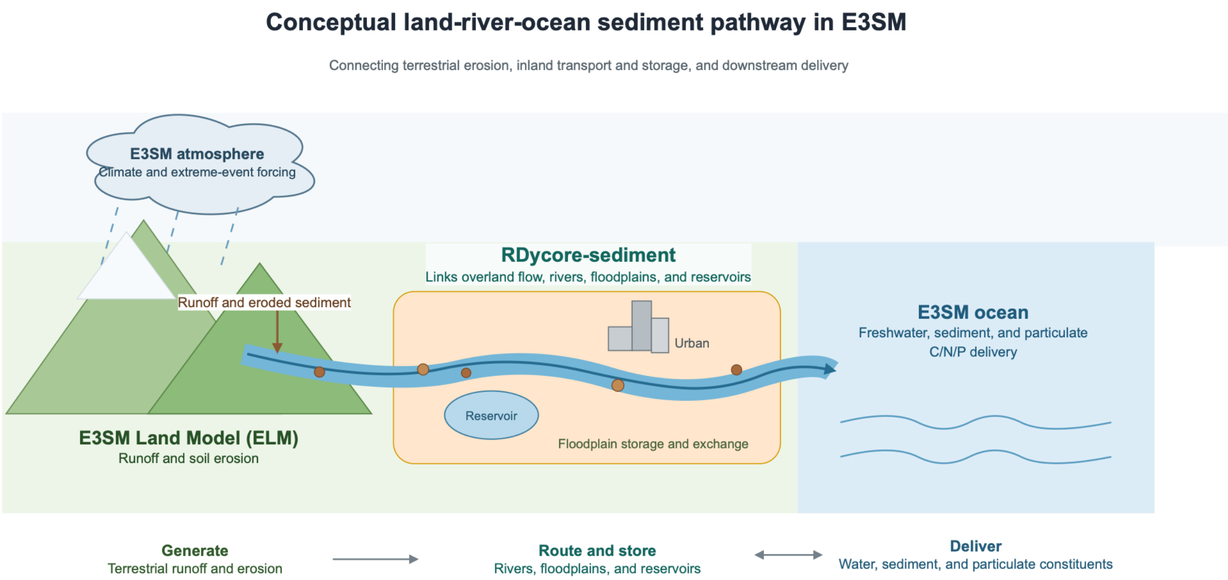

Figure 1: Conceptual source-to-ocean sediment pathway enabled by future integration of RDycore-sediment within E3SM. Atmospheric forcing drives runoff and soil erosion in ELM, while RDycore-sediment routes water, sediment, and particle-associated carbon, nitrogen, and phosphorus through overland-flow, river, floodplain, and reservoir environments before downstream delivery to E3SM ocean components. RDycore-sediment v1.0 currently operates as a standalone model.

2 Methods

RDycore-sediment extends RDycore by adding multi-class depth-averaged suspended sediment transport and cell-local water-bed exchange to its two-dimensional shallow-water formulation. When sediment classes are enabled, RDycore uses tracer-coupled finite-volume operators whose prognostic state includes water depth, momentum, and class-specific suspended sediment mass. The hydrodynamic flux components are computed from the shallow-water variables, while the sediment fluxes are computed from the hydrodynamic mass flux using an upwind sediment concentration. Bed erosion, deposition, and external sediment inputs from hillslope erosion are then applied through the sediment source operator. The coupling is one-way in the present implementation: hydrodynamics control sediment transport and bed exchange through runoff, velocity, depth, and bed shear stress, but sediment does not feed back onto the hydrodynamic solution through morphodynamic bed elevation change (Tassi et al., 2023). RDycore-sediment can be operated as a standalone model driven by runoff and soil erosion fields generated by ELM. The following sections describe the governing equations, bed exchange physics, and numerical scheme.

https://doi.org/10.5194/egusphere-2026-4859
Preprint. Discussion started: 20 August 2026

2.1 Governing equations

RDycore-sediment extends the 2-D shallow water equation system in RDycore by adding multiple suspended sediment classes as conservative tracers in advection transport equation. The hydrodynamic prognostic variables are water depth h and depth-integrated momentum hu and hv, where u and v are the depth-averaged velocities in the x and y directions. For sediment class $s = 1, \dots, N_s$, the prognostic sediment variable is

$$m_s = hc_s, \quad (1)$$

where c_s is the depth-averaged suspended sediment concentration (SSC) of class s. The model state vector is therefore

$$\mathbf{U} = \left[h,\ hu,\ hv,\ m_1,\ m_2,\ \dots,\ m_{N_s}\right]^T, \quad (2)$$

The hydrodynamic equations are the two-dimensional shallow-water equations,

$$\frac{\partial h}{\partial t} + \frac{\partial (hu)}{\partial x} + \frac{\partial (hv)}{\partial y} = S_h, \quad (3)$$

$$\frac{\partial (hu)}{\partial t} + \frac{\partial}{\partial x}\left(hu^2 + \frac{1}{2}gh^2\right) + \frac{\partial}{\partial y}(huv) = -gh\frac{\partial z_b}{\partial x} - \frac{\tau_{bx}}{\rho_w} + S_{hu}\ , \quad (4)$$

$$\frac{\partial (hv)}{\partial t} + \frac{\partial}{\partial x}(huv) + \frac{\partial}{\partial y}\left(hv^2 + \frac{1}{2}gh^2\right) = -gh\frac{\partial z_b}{\partial y} - \frac{\tau_{by}}{\rho_w} + S_{hv}\ . \quad (5)$$

Here z_b is the fixed bed elevation, g is gravitational acceleration, $\rho_w = 1000$ kg m^{-3} is water density, S_h, S_{hu}, and S_{hv} are externally prescribed water and momentum source terms, and τ_{bx} and τ_{by} are the bed friction terms.

For each sediment class, RDycore-sediment solves a conservative suspended sediment transport equation,

$$\frac{\partial m_s}{\partial t} + \frac{\partial (um_s)}{\partial x} + \frac{\partial (vm_s)}{\partial y} = E_s - D_s + S_{m_s}, \qquad s = 1, \dots, N_s. \quad (6)$$

Here E_s is the erosion flux from the bed to the water column, D_s is the deposition flux from the water column to the bed, and S_{m_s} is an optional external sediment source. The current implementation is one-way coupled: h, hu, and hv affect sediment transport and bed exchange, but sediment does not feed back to the hydrodynamic equations.

2.2 Bed exchange

RDycore-sediment uses a cell-local bed model with an active layer and one or up to 32 substrate layers. For sediment class s in bed layer l, the stored bed variable is the layer mass per unit horizontal area, $M_{\ell,s}$ kg m^{-2}. The total mass in layer l is

$$M_\ell = \sum_{s=1}^{N_s} M_{\ell,s}. \quad (7)$$

Bed erosion follows a Partheniades-type excess shear formulation, and deposition follows a settling velocity formulation. The class-specific net bed exchange flux is

$$F_s^{\text{net}} = E_s - D_s. \quad (8)$$

Positive F_s^{net} means net erosion into the water column, and negative F_s^{net} means net deposition to the bed. The implementation applies a positivity limiter so deposition cannot remove more suspended sediment than what is present in the water column:

$$F_s^{\text{net}} \geq -\frac{m_s}{\Delta t}. \quad (9)$$

https://doi.org/10.5194/egusphere-2026-4859
Preprint. Discussion started: 20 August 2026

The bed exchange source term in the suspended sediment equation is therefore

$$\left.\frac{\partial m_s}{\partial t}\right|_{\text{bed}} = F_s^{\text{net}}. \quad (10)$$

Details of the erosion, deposition, active layer update, and bed mass tracking are given in Appendix A1~A3.

2.3 Numerical scheme

RDycore-sediment uses the same cell-centered finite-volume mesh as RDycore. For cell i with area A_i, the semi-discrete update is

$$\frac{d\mathbf{U}_i}{dt} = -\frac{1}{A_i}\sum_{e\in\partial i} \sigma_{i,e}\, L_e \hat{\mathbf{F}}_e + \mathbf{S}_i, \quad (11)$$

where L_e is edge length, $\sigma_{i,e}$ accounts for orientation of edge e relative to cell i, $\hat{\mathbf{F}}_e$ is the numerical flux, and $\mathbf{S}_i$ contains bed slope, friction, external sources, and sediment bed exchange.

At each edge, RDycore first computes the shallow water Roe flux, $\hat{F}_h^{\text{Roe}}$, from the hydrodynamic variables only. The sediment flux, $\hat{F}_{m_s}$, is then evaluated using an upwind concentration selected from the sign of the numerical water flux,

$$c_s^{\text{up}} = \begin{cases} c_{s,L}, & \hat{F}_h^{\text{Roe}} \geq 0, \\ c_{s,R}, & \hat{F}_h^{\text{Roe}} < 0, \end{cases} \quad (12)$$

$$\hat{F}_{m_s} = \hat{F}_h^{\text{Roe}} c_s^{\text{up}}. \quad (13)$$

This upwind sediment-transport scheme is conservative for the transported sediment mass $m_s = hc_s$. Because the Roe water flux and momentum fluxes are computed before sediment concentrations are used, sediment transport does not alter the hydrodynamic fields.

RDycore-sediment applies the hydrodynamic boundary condition to the conservative shallow water variables (i.e., h, hu, hv) and applies sediment boundary conditions through the conservative tracer variable (hc_s). RDycore-sediment currently supports prescribed sediment concentration as a Dirichlet boundary condition. The prescribed sediment concentration values are specified in the input file, and internally converted to the conserved variable, hc, using the boundary water depth values.

In addition to the sediment extension, this work incorporates hydrostatic reconstruction into the finite-volume RDycore shallow water solver. Hydrostatic reconstruction was not available in RDycore v1.0, and its inclusion here improves the well-balanced treatment of wetting and drying and steep bed gradients, which is especially important for sediment transport because small hydrodynamic errors can be amplified through shear-stress-dependent erosion and deposition. At each cell edge, the left and right water depths are reconstructed from the local free-surface elevations and the higher bed elevation of the two neighboring cells. The reconstructed states are then used in the Roe flux calculation, with hydrostatic pressure corrections applied to the momentum equations. This treatment balances the pressure gradient and bed slope terms and is important because the resulting velocity and bed shear stress directly control sediment advection, erosion, and deposition.

Additional details on the Roe flux, wet-dry treatment, hydrostatic reconstruction, and boundary fluxes are provided in Appendix A4~A7.

https://doi.org/10.5194/egusphere-2026-4859
Preprint. Discussion started: 20 August 2026

3 Evaluation cases

An evaluation suite is designed to test RDycore-sediment progressively, from conservative passive transport to source-term verification and a real-event comparison against TELEMAC/GAIA. The first two cases isolate the sediment advection scheme with erosion and deposition disabled. The third case activates water-bed exchange in a controlled dam-break configuration. The fourth case verifies the multi-class sediment implementation with a method of manufactured solutions (MMS). The fifth case evaluates the model in the intended flood application setting by comparing RDycore-sediment and TELEMAC/GAIA for Hurricane Harvey in Houston.

3.1 Passive Sediment Transport Tests

The first two tests reproduce the convective-step sediment transport tests of (Le et al., 2015), which were originally designed to verify passive pollutant transport coupled to shallow water flow (Audusse & Bristeau, 2003). In these tests, bed exchange is disabled so that the sediment equation reduces to conservative advection by the hydrodynamic field. In RDycore-sediment, deposition is disabled by setting the critical deposition shear stress ($\tau_{d,s}$) to zero, and erosion is disabled by setting the Partheniades coefficient ($K_{p,l}$) to zero.

3.1.1 Dam-break passive transport

The first passive case is a one-dimensional dam-break problem on a flat bed with different initial SSCs on each side of the dam. The domain length is 2000 m long with grid spacing $\Delta x = 1$ m. The RDycore mesh has one row in the y direction, and each x interval is divided into four triangular cells. The dam is initially located at the center of the domain, x=1000 m. The left state is

$$h_L = 1 \text{ m}, \qquad u_L = 0, \qquad c_L = 0.7, \tag{14}$$

and the right state is

$$h_R = 0.5 \text{ m}, \qquad u_R = 0, \qquad c_R = 0.5. \tag{15}$$

The bed is flat and Manning friction is set to zero. The analytical shallow water solution contains a rarefaction wave, a shock wave, and a contact discontinuity. The sediment concentration is moved with the flow and changes discontinuously across the contact wave while remaining unchanged across the nonlinear water waves. This makes the case useful for testing whether the sediment upwind scheme captures the correct advective behavior.

The RDycore-sediment setup uses one sediment class, hydrostatic reconstruction, a time step of 0.01 s, and a final time of 240 s. The comparison is the water depth and SSC at 240 s against the analytical Riemann solution. The analytical water depth solution is generated from the classical wet-bed dam-break solution (Stoker, 2019). The reference arrays used for comparison are produced with the MATLAB implementation (Sarkhosh, 2021), and the SSC reference follows the passive-contact solution (Le et al., 2015).

https://doi.org/10.5194/egusphere-2026-4859
Preprint. Discussion started: 20 August 2026

3.1.2 Lake-at-rest test

The second passive case tests preservation of a steady lake-at-rest state over nonflat topography. The computational domain is 20 m long with grid spacing $\Delta x = 0.1$ m, using the same one-row triangular mesh construction as the dam-break case. The exact solution satisfies

$$h + z_b = 1, \qquad u = 0, \tag{16}$$

with a spatially discontinuous initial SSC field, which is set to $c = 1$ g/L over the bump region $8 < x < 12$ and $c = 0$ g/L elsewhere. Because the velocity is zero and diffusion is not considered in the model, the simulated sediment transport should be zero and the simulated SSC should remain unchanged across the entire simulation. This case tests both hydrodynamic well balancing and passive-sediment consistency. The numerical method should preserve the free surface and avoid generating spurious sediment transport.

The RDycore-sediment setup follows the lake-at-rest configuration (Le et al., 2015). It uses one sediment class, hydrostatic reconstruction, zero Manning friction, a time step of 0.0025 s, and a final time of 100 s. Erosion and deposition are disabled as in the passive dam-break case. We compare the free-surface elevation and SSC between RDycore-sediment and analytical solutions.

3.2 Dam break with erosion and deposition

The third case uses the same dam-break configuration as Sect. 3.1.1 but activates bed exchange. This test evaluates whether RDycore-sediment can compute shear stress dependent erosion, settling-velocity-dependent deposition, active-layer mass exchange, and class-specific net bed fluxes in a transient flow. This test attempts to reproduce the suspended sediment response produced by TELEMAC/GAIA when both models are configured with the same sediment parameters and hydrodynamic forcing. Unlike the passive tests, the SSC field in this case evolves through both advective transport and local water-bed exchange.

The RDycore-sediment setup uses one sediment class with density 1600 kg m^{-3}, settling velocity 1×10^{-4} m s^{-1}, and critical deposition shear stress 0.1 N m^{-2}. The active-layer thickness is 0.1 m. The substrate layer has initial thickness 0.1 m, concentration 100 kg m^{-3}, Partheniades coefficient 1.0×10^{-4} kg m^{-2} s^{-1}, and critical erosion shear stress 0.1 N m^{-2}. Manning roughness is set to n=0.025. The simulation uses hydrostatic reconstruction, a time step of 0.01 s, and a final time of 240 s. The same mesh and initial water/sediment files used by the passive dam-break case are used here. Since RDycore-sediment does not update bed elevation in this version, the comparison focuses on water-column concentration rather than morphodynamic change. We compare water depth, SSC, and bottom shear stress.

3.3 Method of Manufactured Solutions

The fourth case verifies the coupled transport and bed exchange implementation using the MMS approach (Steinberg & Roache, 1985). MMS verifies the numerical implementation by prescribing smooth analytical solutions for the model variables

https://doi.org/10.5194/egusphere-2026-4859
Preprint. Discussion started: 20 August 2026

and parameters, deriving the corresponding boundary conditions and source terms, and comparing the numerical solution against the manufactured solution. The hydrodynamic part of the test follows the RDycore MMS configuration (Bisht et al., 2025), including the manufactured water depth, velocity, bed elevation, Manning coefficient, source-term construction, and grid-refinement setup. We extend that setup by prescribing three manufactured SSC fields and by adding the corresponding class-wise source terms to the sediment transport equations.

The three sediment classes use parameter values representative of the Hurricane Harvey TELEMAC/GAIA application (Feng et al., 2026), including different settling velocities, critical deposition stresses, sediment densities, Partheniades erosion coefficients, critical erosion stresses, and bed layer sediment concentrations. The MMS therefore verifies the sediment advection, water column SSC evolution, and erosion-deposition source-term coupling under spatially and temporally varying hydrodynamic conditions. The sediment manufactured solutions and the resulting source terms are given in Appendix B.

Numerical errors are evaluated by comparing the simulated conservative sediment variables m_s with the corresponding manufactured solutions on successively refined meshes. This test is used to confirm that the sediment transport and bed exchange implementation produce the expected convergence behavior when the exact sediment solution is known. The convergence test starts from the triangular MMS mesh (Bisht et al., 2025). Following the MMS refinement settings, the mesh is uniformly refined from refinement level 1 to level 4, giving nominal grid spacings of 0.5, 0.25, 0.125, and 0.0625 m. We evaluate numerical accuracy and convergence using three cell-area-weighted error norms (L_1, L_2, and L_∞) defined in Appendix B.

3.4 Hurricane Harvey Houston simulation

The fifth test evaluates RDycore-sediment against the TELEMAC/GAIA benchmark simulation (SED-1) of Feng et al. (2026) for the Hurricane Harvey flood event in Houston. This test evaluates whether RDycore-sediment can reproduce the hydrodynamic and suspended sediment response of an established process-based benchmark under consistent forcing and sediment parameters. It also examines the model's suitability for regional flood-sediment applications and identifies the limitation of neglecting bed evolution in the current implementation.

The domain is the Turning Basin portion of the Buffalo Bayou watershed (Fig. 2), extending from the upstream reaches of Addicks and Barker reservoirs to the Buffalo Bayou outlet. In Feng et al. (2026), the TELEMAC/GAIA benchmark used a Delaunay-based unstructured mesh, with bottom elevation resampled from the 30 m National Elevation Dataset DEM. The mesh is refined to approximately 30 m along the main channel floodplain, Addicks and Barker reservoir areas, approximately 90 m along tributary floodplains, and approximately 1000 m in areas away from the floodplain and reservoir features, resulting in 442,277 triangular cells. The RDycore-sediment simulation uses the same Houston benchmark domain, downstream boundary forcing, sediment parameters, and ELM-derived runoff and hillslope erosion inputs used for the TELEMAC/GAIA comparison. ELM is driven by Multi-Radar Multi-Sensor System (MRMS) Gauge-Corrected Quantitative Precipitation Estimate 1 h precipitation and NLDAS atmospheric forcing. ELM provided hourly spatially distributed runoff and hillslope soil erosion fluxes. In RDycore-sediment, runoff is applied as a water source term (Eq. 3), while the ELM-derived hillslope

https://doi.org/10.5194/egusphere-2026-4859
Preprint. Discussion started: 20 August 2026

erosion flux is applied as an external source in the conservative suspended sediment equation (Eq. 6). The downstream open boundary is prescribed using observed water level from the NOAA Manchester, TX tide gauge (station 8770777), and the simulation uses the same spatially uniform Manning roughness value, n=0.015. The sediment setup follows the three-class configuration with two hillslope-derived classes and a third coarser bed material class. The initial bed composition fractions are 0.3, 0.3, and 0.4 for the three classes, respectively.

The comparison focuses on water stage and SSC at 16 USGS gauge locations distributed across the domain, which are used to evaluate whether RDycore-sediment reproduces the timing, magnitude, and recession behavior of the benchmark simulation during the flood event. In addition, we compare bulk deposition behavior over four distinct regions: Addicks Reservoir, Barker Reservoir, Buffalo Bayou, and White Oak Bayou. These regional comparisons provide a spatially aggregated measure of sediment retention and erosion-deposition behavior in reservoirs and major channel corridors. For TELEMAC/GAIA, the regional deposition quantity is estimated from simulated bed elevation change. In contrast, RDycore-sediment deposition is estimated diagnostically from the output net erosion-deposition flux (F_s^{net}). This RDycore diagnostic should be interpreted as an approximation of potential net deposition or erosion, rather than as a true morphodynamic bed change prediction.

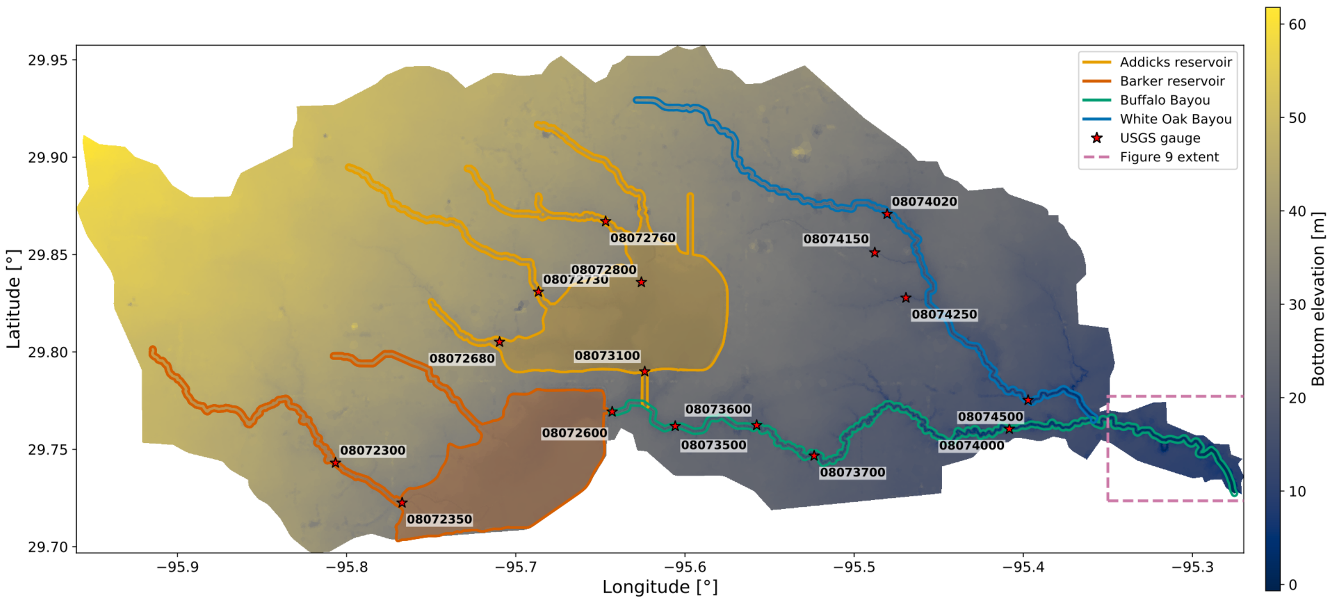

Figure 2: RDycore bottom elevation across the Houston model domain. Red stars indicate the 16 USGS gauge locations, while colored outlines delineate the Addicks Reservoir, Barker Reservoir, Buffalo Bayou, and White Oak Bayou regions used for sediment-mass calculations.

https://doi.org/10.5194/egusphere-2026-4859
Preprint. Discussion started: 20 August 2026

4 Results

4.1 Passive sediment transport tests

In the dam-break test, RDycore-sediment accurately reproduces the analytical solution of water surface elevation and SSC at the final time step (Fig. 3a and 3c). The numerical and analytical solutions are consistent for both variables, including the sharp hydraulic transitions and the associated SSC discontinuity. This agreement indicates that the upwind sediment flux follows the hydrodynamic mass flux consistently. The lake-at-rest test further confirms that the sediment transport scheme preserves a stationary sediment field under zero-flow conditions over variable topography (Fig. 3b and 3d). The water surface remains horizontal across the immersed bump, and the final SSC distribution remains almost identical to the analytical solution.

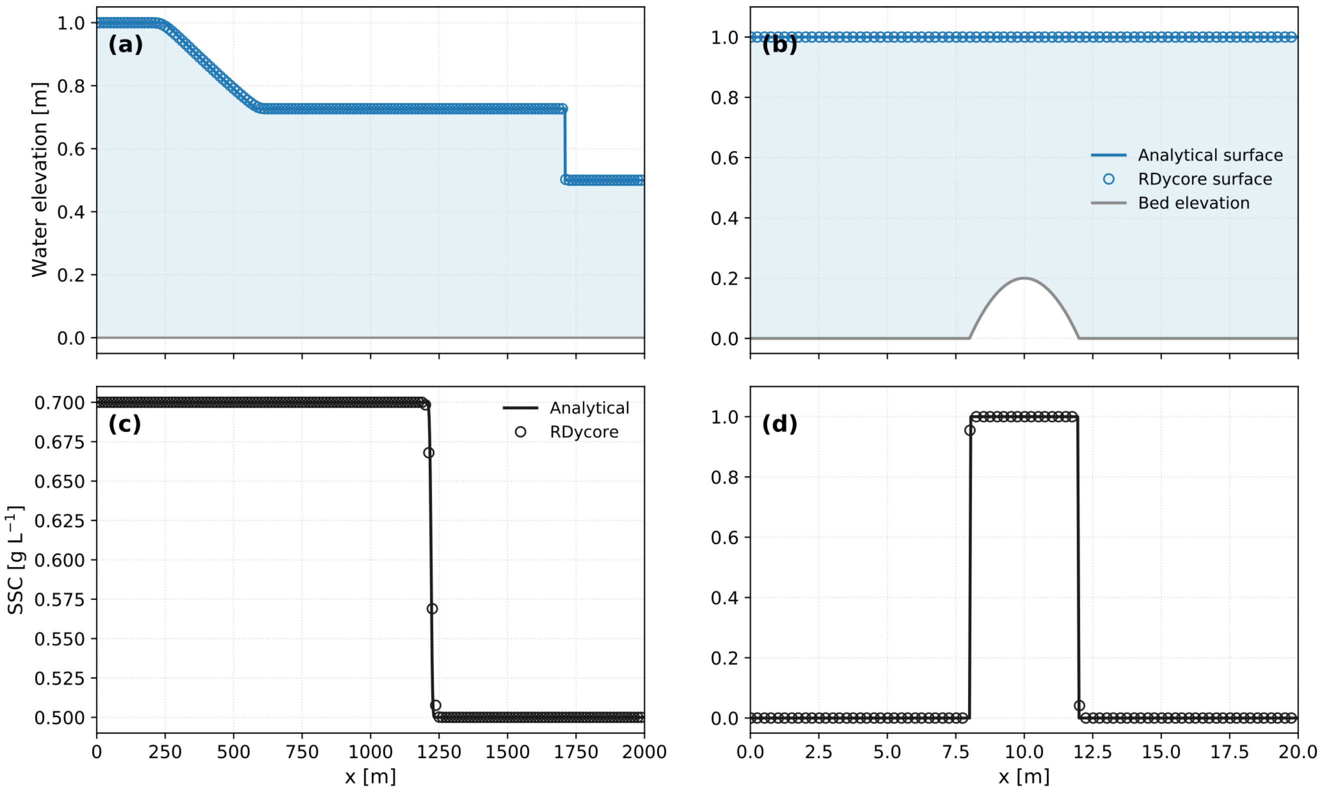

Figure 3: Passive sediment transport verification for RDycore-sediment. Dam-break test comparing (a) water surface elevation and (c) suspended sediment concentration (SSC) from RDycore-sediment with the analytical solution at the final time step. Lake-at-rest test comparing (b) water surface elevation and (d) SSC from RDycore-sediment with the analytical solution at the final time step. Bottom elevation with the immersed bump is also shown.

4.2 Dam break with erosion and deposition

RDycore-sediment produces water depth, bed shear stress, and SSC patterns that are consistent with the TELEMAC/GAIA benchmark at the final time step (Fig. 4). The water depth comparison indicates that the hydrodynamic solutions of the two models remain closely aligned after adding sediment source terms. The bed shear stress fields also show consistent spatial

https://doi.org/10.5194/egusphere-2026-4859
Preprint. Discussion started: 20 August 2026

structure between the two models, which is important because shear stress controls the onset and magnitude of erosion and deposition. The SSC comparison shows that RDycore-sediment simulates the main sediment response of the dam-break flow reasonably. Elevated SSC occurs in regions where the dam-break wave generates stronger bed shear stress, while lower SSC occurs in relatively quiescent regions where deposition is favored. The agreement with TELEMAC/GAIA demonstrates that the implemented erosion and deposition terms produce physically consistent sediment exchange under rapidly varying flow conditions.

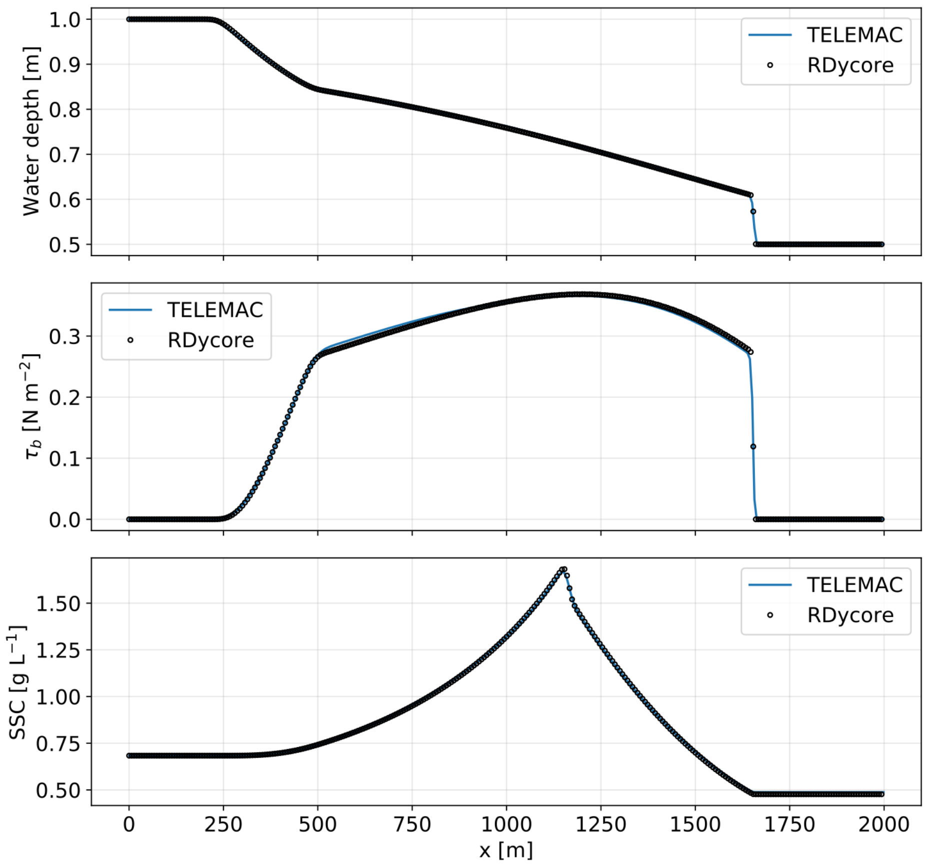

Figure 4: Dam-break test with erosion and deposition comparing TELEMAC/GAIA and RDycore-sediment at the final time step. The panels show water depth, bottom shear stress, and suspended sediment concentration (SSC).

4.3 Method of manufactured solutions

The L_1, L_2, and L_∞ errors in the MMS test decrease monotonically as the nominal grid spacing decreases from 0.5 to 0.0625 m (Fig. 5). The hydrodynamic variables retain the convergence behavior previously reported for RDycore (Bisht et al., 2025). These results confirm that introducing sediment transport and bed exchange calculations does not change the hydrodynamic solution. This behavior is consistent with the one-way coupling implemented in RDycore-sediment, in which the upwind sediment flux uses the hydrodynamic mass flux but does not modify the water depth or momentum fields. The conservative

https://doi.org/10.5194/egusphere-2026-4859
Preprint. Discussion started: 20 August 2026

sediment variables also show approximately first-order convergence (>0.94). The consistent convergence across the three sediment classes highlights the robustness of the numerical implementation of sediment advection and the associated erosion-deposition source terms.

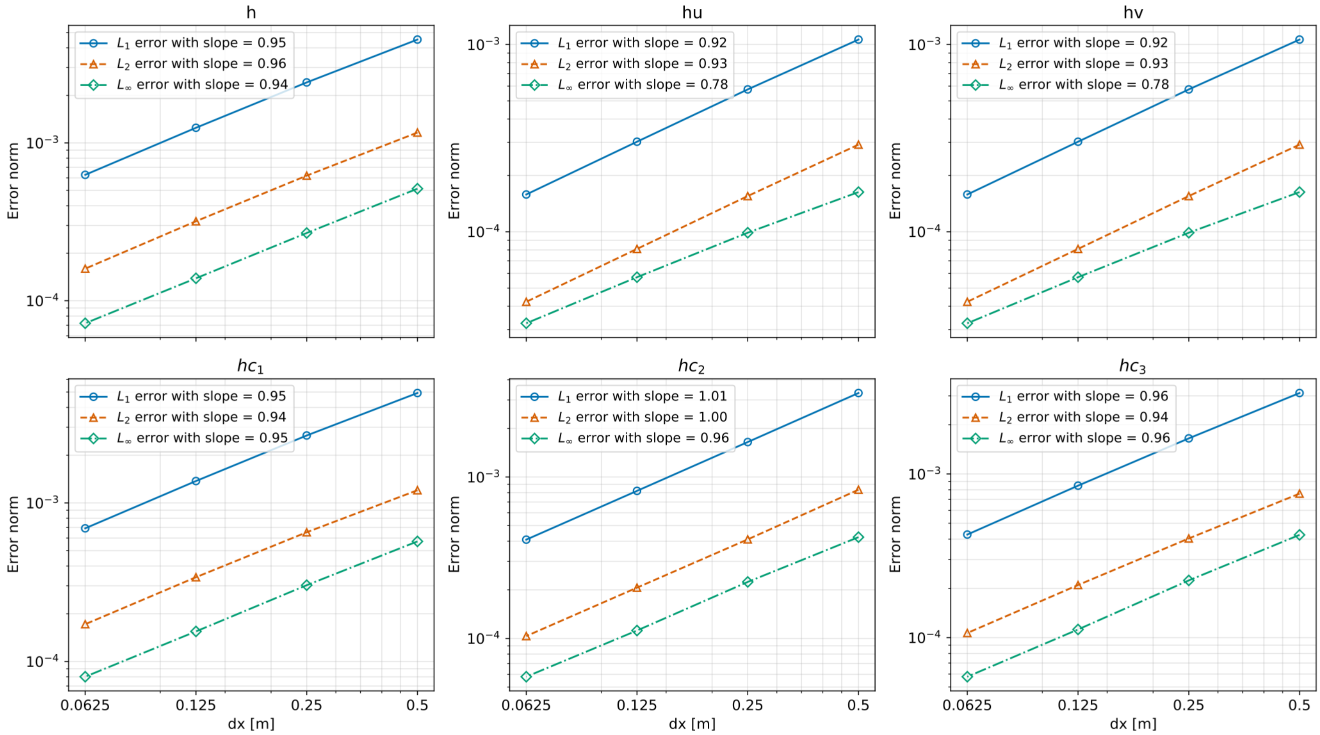

Figure 5: Grid convergence of the cell-area-weighted L_1, L_2, and L_∞ errors at $t = 5$ s for the hydrodynamic variables h, hu, hv, and conservative sediment variables hc_1, hc_2, and hc_3 with grid spacing from 0.0625, 0.125, 0.25, and 0.5 m. Slope represents first-order convergence rate.

4.4 Harvey simulation

RDycore-sediment reproduces the main hydrodynamic behavior of the TELEMAC/GAIA benchmark across the 16 USGS gauge locations (Fig. 6). The timing of the flood rise, major peaks, and recession is generally consistent between the two models. The model discrepancies relative to the USGS stage observations are similar for RDycore and TELEMAC/GAIA. Differences between the two model simulations are partly associated with that bed elevation changes are represented in TELEMAC/GAIA but not in the current RDycore-sediment (Fig. S1).

The spatiotemporal variability of the simulated SSC is also generally consistent between RDycore-sediment and TELEMAC/GAIA while substantial differences in magnitude exist (Fig. 7). Both models simulate low SSC before the main rainfall-runoff response, followed by rapid increases during the flood rise and elevated SSCs during the peak-flow period. RDycore-sediment captures the timing of the main SSC pulses at most stations and reproduces the order of magnitude of the

https://doi.org/10.5194/egusphere-2026-4859
Preprint. Discussion started: 20 August 2026

TELEMAC/GAIA SSCs. At two gauges (i.e., 08073700 and 08074000), RDycore simulates sharper and higher short-duration SSC peaks that do not appear in the TELEMAC/GAIA simulation. This divergence mainly reflects the differences of the two models in coupling with hillslope sediment inputs and managing bed exchange. RDycore-sediment applies the ELM-derived erosion input directly in the source term of the sediment transport equation together with local bed erosion and deposition (Eq. 6), whereas TELEMAC/GAIA solves for suspended sediment through a split sequence in which GAIA computes erosion and prepares deposition terms, TELEMAC solves the tracer advection-diffusion/source update, and GAIA then applies deposition and bed evolution. This sequential treatment can smooth the immediate SSC response to large local runoff-driven soil erosion inputs where RDycore simulates sharper local SSC peaks. Moreover, larger differences occur at gauges 08072600 and 08073100, which are located immediately downstream of the Addicks and Barker flood-control reservoir outlets. The previous TELEMAC/GAIA simulation indicated substantial bed elevation changes in these reservoir areas (Feng et al., 2026), with changes exceeding 0.4 m at the exact gauges (Fig. S1). Such morphodynamic adjustment can cause nonlinear effects on both flow routing and sediment transport (Feng et al., 2025) which are not represented in the current RDycore-sediment.

Basin-integrated sediment dynamics show similar temporal variability between the two models (Fig. 8). The bed mass change rates increase rapidly during the main flood response and reach their largest values during August 27-28, when flow discharge and sediment availability are highest. RDycore and TELEMAC/GAIA simulate similar timing and magnitude for the dominant bed exchange pulses. Boundary sediment export also follows the flood hydrograph, with both models predicting the largest export rates near the main discharge peak. In general, RDycore simulates lower deposition rate and higher export rates during parts of the event, but the temporal variation is consistent between the two simulations.

The integrated bed mass diagnostics over the whole event further support the consistency between RDycore-sediment and TELEMAC/GAIA (Table 1). Over the full basin domain, RDycore estimates a total mass increase on riverbed and floodplains of 1.37×10^9 kg, in line with 1.53×10^9 kg from GAIA. Class-specific totals are also comparable, with both models showing net deposition for classes 1 and 2 and net erosion for class 3. Both models predict greater deposition of class 2 than class 1, consistent with the larger particle size and settling velocity of class 2. Regionally, both models simulate net deposition in Addicks and Barker reservoirs and net erosion in Buffalo Bayou. RDycore simulates larger deposition in Barker Reservoir and weaker erosion in Buffalo Bayou. In White Oak Bayou, RDycore simulates a small net erosion whereas TELEMAC/GAIA simulates a small net deposition. This difference is expected to be more sensitive to numerical formulation because White Oak Bayou has narrow channel sections that are locally close to, or below, the effective mesh resolution. The bed mass diagnostics should also be interpreted with some caution because they are computed differently in the two models. As described in Section 3.4, GAIA bed mass change is calculated from the difference between the final and initial layer mass variables, whereas the RDycore diagnostic is reconstructed by time-integrating the output deposition/erosion mass fluxes at each time step.

Note that the considerable differences between the two models are expected because they are independently implemented and an exact analytical solution for the Harvey case is unknown. The main implementation differences are summarized in Table 2. These differences can influence how quickly sediment inputs enter the water column, how long sediment remains suspended in reservoir and channel storage areas with low-velocity flows, and how much material is deposited or remobilized during the

https://doi.org/10.5194/egusphere-2026-4859
Preprint. Discussion started: 20 August 2026

event. Overall, the close agreement in event-scale timing, total bed mass change, and regional erosion and deposition patterns indicates that RDycore-sediment captures the main behavior of the TELEMAC/GAIA benchmark.

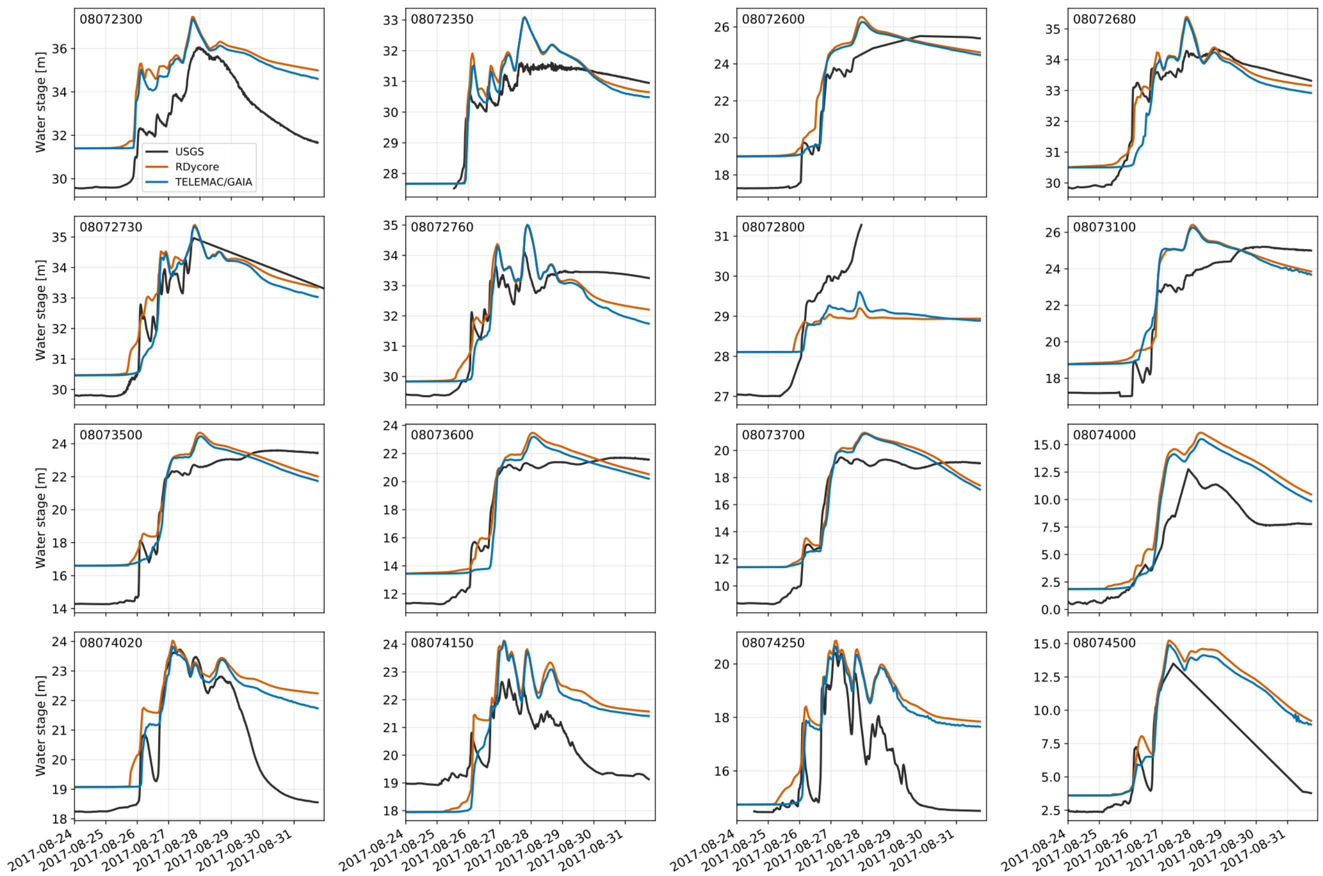

Figure 6: Water-stage comparison at 16 USGS gauge locations during the Hurricane Harvey Houston simulation.

https://doi.org/10.5194/egusphere-2026-4859
Preprint. Discussion started: 20 August 2026

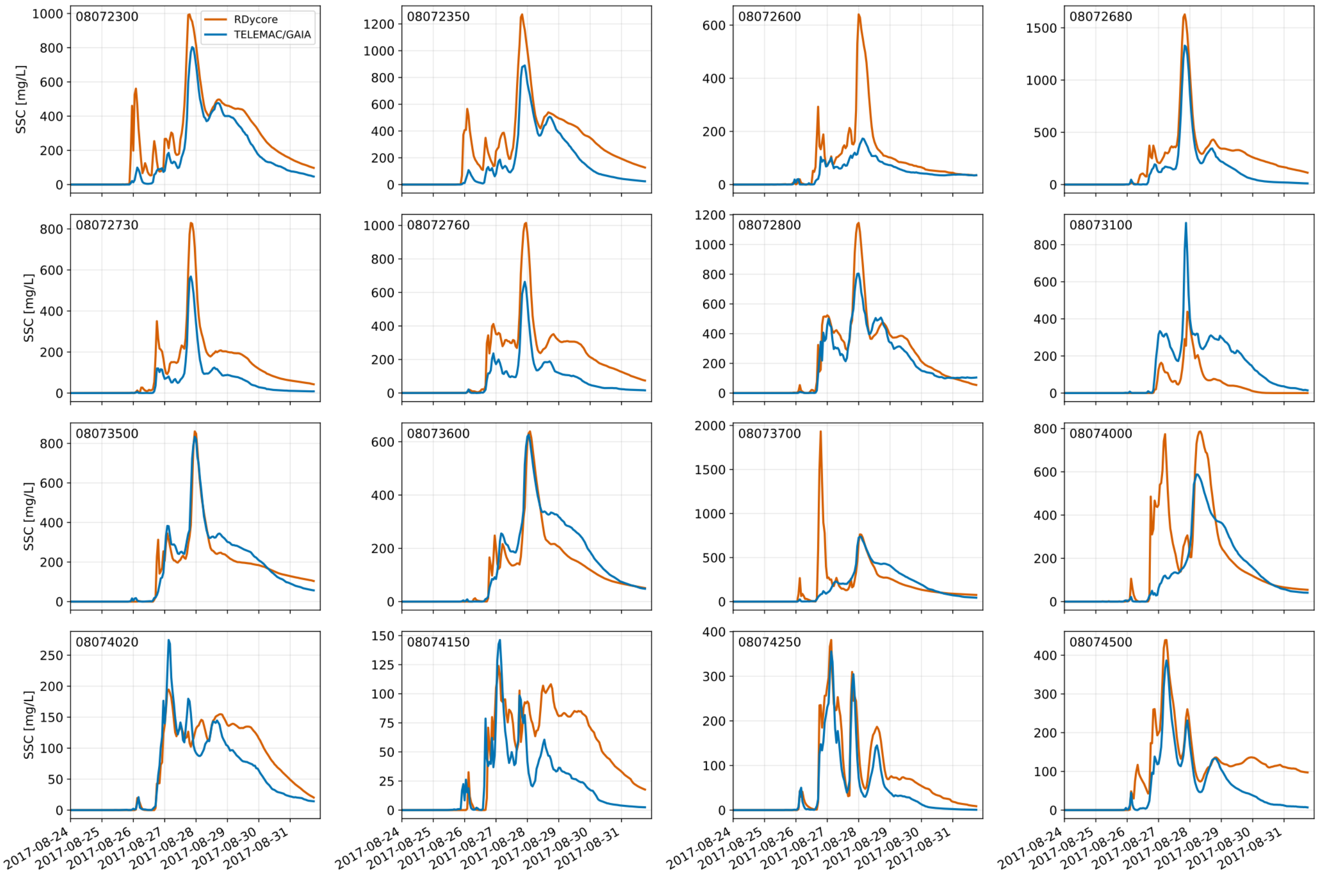

Figure 7: Suspended sediment concentration (SSC) comparison at 16 USGS gauge locations during the Hurricane Harvey Houston simulation.

https://doi.org/10.5194/egusphere-2026-4859
Preprint. Discussion started: 20 August 2026

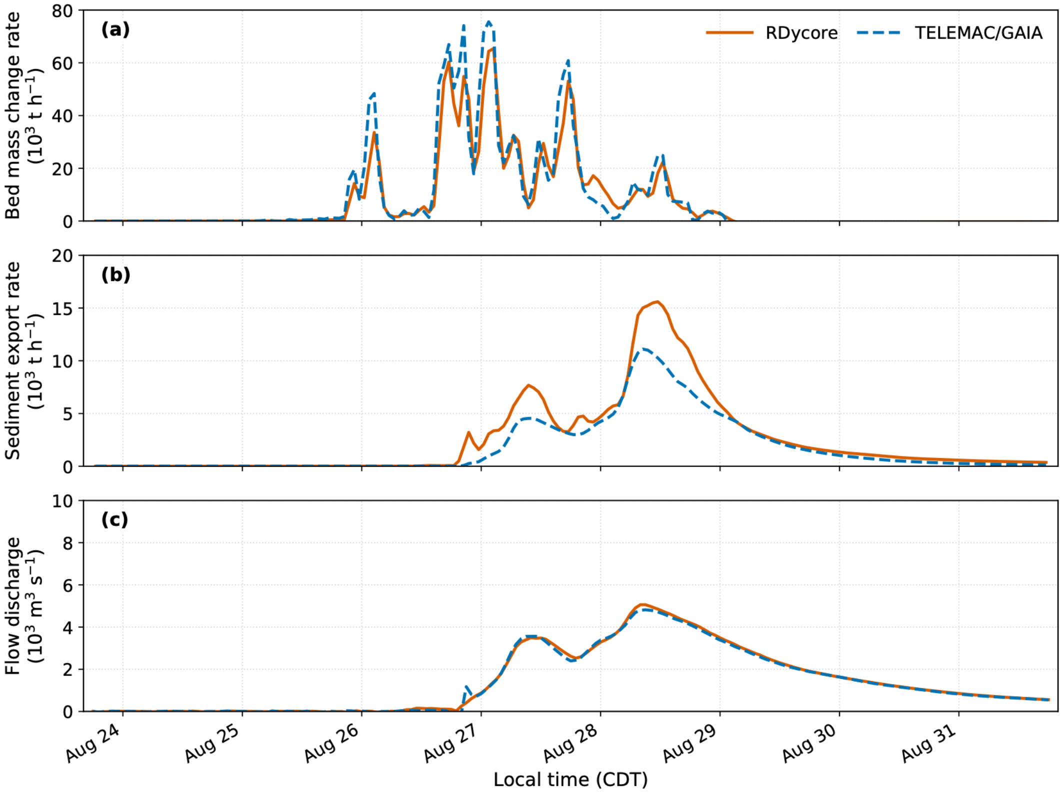

Figure 8: Basin-integrated temporal sediment and flow rate from RDycore-sediment and TELEMAC/GAIA: (a) bed mass change rate. (b) Downstream boundary sediment export rate, and (c) flow discharge. Positive bed mass change indicates net deposition.

Table 1. Integrated bed mass change from RDycore-sediment and TELEMAC/GAIA during the Hurricane Harvey Houston simulation. Positive values indicate net deposition, and negative values indicate net erosion. Values are reported in 10^8 kg.

	RDycore	**TELEMAC/GAIA**
Total basin domain	13.8	15.4
Class 1	5.5	6.7
Class 2	9.1	10.0
Class 3	-0.77	-1.29
Addicks Reservoir	0.90	0.92
Barker Reservoir	2.68	1.62
Buffalo Bayou	-0.78	-1.63
White Oak Bayou	-0.01	0.08

https://doi.org/10.5194/egusphere-2026-4859
Preprint. Discussion started: 20 August 2026

Table 2. Model implementation differences between RDycore-sediment and TELEMAC/GAIA in the Hurricane Harvey simulation.

Component	RDycore-sediment	TELEMAC/GAIA
Hydrodynamics	Cell-centered finite volume shallow water solver	Node-based finite element shallow water solver
Source term treatment	External ELM soil erosion, bed erosion, and deposition all applied in the sediment source update	Fractional step sequence: GAIA computes bed erosion and deposition terms, TELEMAC transports suspended sediment with the ELM soil erosion source, and GAIA updates bed exchange
Hillslope sediment input	ELM soil erosion enters directly as an external source in the conservative sediment equation	Hillslope input enters through the TELEMAC/GAIA split sediment workflow
Morphodynamic feedback	Not included	Included through bed elevation change
Bed mass diagnostic	Time-integrated RDycore erosion/deposition flux outputs	Difference between final and initial GAIA bed-layer mass variables

5 Discussion

5.1 Computational performance

Computational efficiency is central to the intended use of RDycore-sediment within E3SM, which aims to route sediment across large rivers, floodplains, and coastal interfaces together with hydrologic and biogeochemical fluxes. The Hurricane Harvey case provides a practical estimate of the additional cost introduced by the sediment module in an event-scale simulation. On two dual-socket CPU nodes, equipped with four AMD EPYC 7763 (Milan) processors and 256 physical CPU cores in total, the hydrodynamic-only simulation took about 50 min. Using the same computational resources, adding sediment transport and bed exchange increased the runtime to about 1 h 20 min, and including offline ELM-derived hillslope erosion input increased it further to about 1 h 50 min. In comparison, the TELEMAC/GAIA benchmark required 11 h 44 min on one Perlmutter node and 47 h on two nodes for the same configuration. Although these timings are practical configuration-specific comparisons rather than optimized scaling benchmarks, they illustrate an important benefit for RDycore-sediment: RDycore is designed for scalable execution on modern high-performance computing systems, whereas established morphodynamic models such as TELEMAC/GAIA can be more difficult to scale efficiently for large-domain Earth system applications.

The added sediment cost remains moderate relative to the hydrodynamic solver. The increase from 1 h 20 min to 1 h 50 min is mainly associated with offline forcing input rather than the sediment equations themselves. In the present standalone configuration, high-resolution ELM erosion fields are read from external files at hourly intervals for three sediment classes, requiring three large input files at each forcing time. This overhead depends on file size, file layout, storage location, and filesystem throughput. In future online ELM-RDycore coupling, these sediment source fields would be exchanged in memory rather than repeatedly read from disk, so this portion of the cost is expected to decrease.

https://doi.org/10.5194/egusphere-2026-4859
Preprint. Discussion started: 20 August 2026

We did not perform a formal scalability assessment for the Harvey sediment case because the problem size is relatively small compared with the RDycore simulations used to evaluate scalability in Bisht et al. (2025). The one-, two-, and four-node timings should therefore be interpreted as a limited node-count sensitivity for this event setup. The weak improvement beyond two nodes likely reflects the modest Harvey mesh size together with the offline input overhead. Larger source-to-ocean applications will be needed to quantify the scalability of RDycore-sediment under the problem sizes targeted for E3SM.

5.2 Hydrostatic reconstruction

Hydrostatic reconstruction is essential for stability in RDycore-sediment, although its effect on simulated water stage appears small. In the no-hydrostatic-reconstruction experiment, water stage at the 16 USGS gauges remains reasonable in the Hurricane Harvey simulation (Fig. S2), but the simulated SSC and bottom shear stress (τ_b) are substantially degraded (Figs. S3 and S4). This is because small spurious oscillations in water stage can generate much larger oscillations in τ_b, producing unphysical SSC peaks that coincide with the onset of runoff input to the domain. These results indicate that hydrodynamic errors affect the sediment solution not only through transport fluxes, but also through the shear stress dependent erosion and deposition terms. Reducing the model time step from 0.5 s to 0.01 s does not remove this erroneous behavior. As described in Sect. 2.3 and Appendix A5, hydrostatic reconstruction is designed to preserve well-balanced hydrodynamics over irregular topography. This sensitivity test underscores the importance of the well-balanced hydrostatic reconstruction for the Harvey case as it features complex urban topographic features and wetting-drying fronts and in which small imbalances between pressure gradient and bed slope terms can cause locally erroneous momentum and velocity.

Therefore, hydrostatic reconstruction is not only a hydrodynamic stabilization choice but also a necessary component of the sediment model. The issue is specific to the finite-volume RDycore configuration tested here, whereas TELEMAC/GAIA uses a different finite-element hydrodynamic discretization and does not exhibit the same spurious shear stress response in this benchmark. Maintaining a well-balanced finite-volume formulation is therefore required to obtain physically meaningful shear stress and sediment exchange.

5.3 Coastal backwater effects

The downstream water-level boundary condition provides a useful test on how RDycore-sediment responds to elevated coastal water level, which is important because RDycore is intended to be coupled with an ocean model in E3SM. We compare the baseline Harvey simulation, which uses a time-varying ocean water-level boundary, with a control simulation in which the downstream boundary water level is held constant. The fixed value is selected from the pre-Harvey NOAA water-level record at Manchester, TX (station 8770777), using the mean water level from 1 June to 23 August 2017 (Fig. S5).

The spatial comparison shows that the downstream boundary condition can substantially affect local hydrodynamics and sediment dynamics (Fig. 9). The largest differences in water depth occur near the downstream boundary and along connected low-gradient channels and floodplain areas where changes in water-surface elevation modify the local pressure gradient and drainage capacity (Feng et al., 2022). These hydrodynamic changes also affect SSC and cumulative bed mass change. In particular, elevated coastal water levels can reduce downstream conveyance, increase local water depth, modify SSC, and shift where suspended sediment is deposited or remobilized. Elevated downstream water levels reduce local drainage and flow velocity, which induces more sediment deposition. However, the effect on event-scale discharge at the downstream boundary is limited in this Harvey configuration (Fig. S6). The flow-discharge time series from the time-varying and fixed-boundary simulations have nearly the same event timing and peak magnitude. Similarly, the total suspended sediment discharge remains close between the two simulations. These differences are small compared with the event-scale discharge peaks, indicating that discharge in this case is controlled primarily by precipitation-driven runoff, while the coastal boundary condition mainly redistributes water and sediment locally. The influence of coastal backwater may be more important for longer-term simulations or smaller flood events, when tidal and storm-surge variability can represent a larger fraction of the total hydraulic forcing. This sensitivity should be examined in future long-term RDycore-ocean coupled applications.

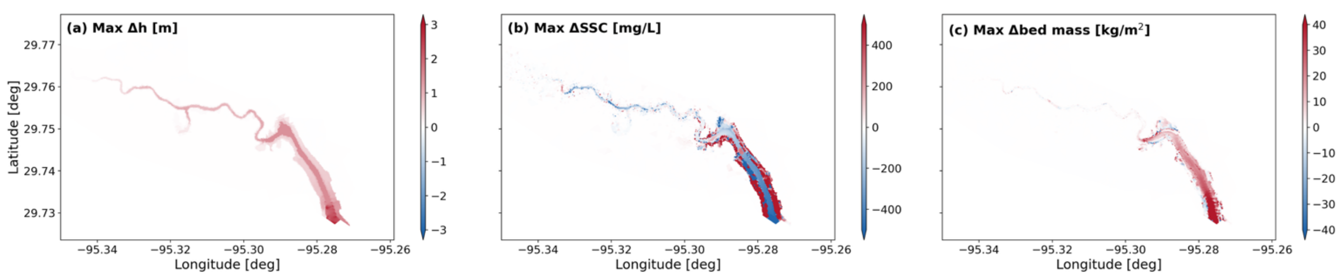

Figure 9: Maximum differences between RDycore simulations with a time-varying ocean water-level boundary and a fixed downstream water-level boundary. Panels show the spatial maximum difference (ocean-fixed) over the simulation period for (a) water depth, (b) suspended sediment concentration (SSC), and (c) cumulative bed sediment mass change. Larger values indicate locations where the ocean boundary condition most strongly modifies hydrodynamics, suspended sediment transport, or net bed sediment exchange. The spatial extent used here is specified in Figure 2.

5.4 Limitations and future work

The present version of RDycore-sediment uses a one-way hydrodynamic-sediment coupling strategy. Sediment does not feed back onto the hydrodynamic components. Bed exchange modifies suspended and bed sediment mass, but it does not change bed elevation or water depth through morphodynamic feedback. Implementing two-way morphodynamic feedback would therefore require coordinated changes to the time integration and operator structure across the relevant RDycore hydrodynamic and sediment-coupled operators.

This choice is intentional for the first RDycore-sediment release. RDycore is designed for large-scale E3SM applications, where simulations may cover complex terrains. In such applications, two-way morphodynamic feedback from bed elevation change to flow depth and momentum can introduce substantial numerical sensitivity. This is also consistent with current river components in Earth system models that assume a constant river channel geometry (Li et al., 2022). We therefore prioritize a stable suspended sediment transport model in which sediment does not feed back onto the hydrodynamic solution. This

https://doi.org/10.5194/egusphere-2026-4859
Preprint. Discussion started: 20 August 2026

behavior is verified for the Harvey case (Fig. S7). The hydrodynamic-only and hydrodynamic-sediment simulations produce nearly identical water depth and velocity fields, with maximum differences of only $O(10^{-6})$ m for water depth and $O(10^{-5})$ m s^{-1} for velocity.

The one-way coupling strategy may limit applications where bed evolution strongly modifies flow routing and sediment transport. Although RDycore-sediment updates bed sediment mass and diagnoses net bed exchange fluxes, it does not solve an Exner equation and assumes mesh bed elevation remains unchanged throughout the simulation. Bed exchange affects suspended sediment mass and local sediment mass stored in the bed, but the resulting erosion or deposition does not modify hydrodynamic conveyance. As discussed in Sect. 4.4, this difference partly explains differences between RDycore-sediment and TELEMAC/GAIA. It also means that the current model cannot represent morphodynamic feedbacks that may become important in sediment-laden environments, where bed elevation change can alter local hydraulics, deposition patterns, and channel or floodplain morphology (Feng et al., 2025).

Future development will focus on adding two-way morphodynamic feedback while preserving RDycore's stability. This will require solving bed elevation evolution consistently with sediment mass exchange and refactoring parts of the RDycore time-integration workflow so that hydrodynamics, sediment transport, and bed evolution can be coupled robustly. A second major next step is integrating RDycore-sediment into E3SM for online coupling, so that hillslope sediment input from ELM can be passed in memory rather than through offline forcing files. The current implementation has been developed and tested for CPU execution. Extending the sediment operators to GPU-enabled RDycore builds is expected to be straightforward, but will require coordination with ongoing RDycore development. Together, these developments will extend RDycore-sediment from a stable suspended sediment routing capability toward a fully coupled land-river-ocean sediment and morphodynamic modeling framework. In addition to sediment, this modeling framework can help advance the predictive understanding of the fate of carbon, nutrients, pollutants, and contaminants in aquatic and coastal systems (Peng et al., 2025; Regnier et al., 2022; Tan et al., 2021).

6 Conclusions

The main contribution of RDycore-sediment is to bridge two existing sediment transport model systems. On one side are Earth system sediment models such as MOSART-sediment that can represent large-scale sediment budgets but cannot resolve 2-D floodplain hydraulics. On the other side are detailed morphodynamic models such as TELEMAC/GAIA that represent bed evolution but are not designed to deploy routinely at Earth-system scales. RDycore-sediment sits in the middle ground: it routes suspended sediment through spatially resolved overland-flow, river, reservoir, and floodplain environments using a computational framework designed for large-scale applications.

The evaluation cases demonstrate the robustness of this new sediment transport model. RDycore-sediment preserves passive sediment transport, reproduces controlled erosion-deposition behavior, converges under manufactured-solution forcing, and captures the main hydrodynamic and suspended sediment behavior of the Hurricane Harvey TELEMAC/GAIA benchmark.

https://doi.org/10.5194/egusphere-2026-4859
Preprint. Discussion started: 20 August 2026

The Harvey results also reveal an important practical lesson that sediment predictions are highly sensitive to hydrodynamic balance because erosion and deposition respond nonlinearly to bed shear stress. Thus, well-balanced hydrodynamics are not only a water-stage requirement, but a prerequisite for physically meaningful sediment exchange.

The current model should not yet be interpreted as a morphodynamic model. Future work should therefore focus on Exner-based bed evolution, two-way morphodynamic feedback, and online E3SM-RDycore coupling so that hillslope erosion, floodplain routing, and downstream particulate delivery can be represented consistently within ESMs.

Appendix A

A1 Bed initialization and layer properties

At initialization, the user provides the class fractions f_s for each sediment class s, which satisfies

$$\sum_{s=1}^{N_s} f_s = 1. \tag{A1}$$

The initial bed mass in layer l is

$$M_{\ell,s}^0 = f_s C_\ell H_\ell. \tag{A2}$$

Here C_l is the layer sediment concentration parameter provided in the input file and H_ℓ is the initial layer thickness. The initial bulk particle density is

$$\rho_{\mathrm{bulk}}^0 = \sum_{s=1}^{N_s} f_s \, \rho_s, \tag{A3}$$

and the model computes a porosity-like layer parameter as

$$\phi_\ell = 1 - \frac{C_\ell}{\rho_{\mathrm{bulk}}^0}. \tag{A4}$$

A2 Erosion and deposition

Manning friction is used to compute bed shear stress. The drag coefficient is

$$C_d = g n^2 h^{-1/3}, \tag{A5}$$

The vector bed shear stress is

$$\boldsymbol{\tau}_b = \rho_w C_d |\mathbf{u}| \mathbf{u}, \tag{A6}$$

where $|\mathbf{u}| = \sqrt{u^2 + v^2}$. The scalar bed shear stress used by the sediment erosion and deposition formulas is

$$\tau_b = \rho_w C_d (u^2 + v^2). \tag{A7}$$

For each sediment class, the user provides particle density ρ_s, settling velocity w_s, and critical deposition shear stress $\tau_{d,s}$. For each substrate layer, the user provides initial thickness, concentration, Partheniades erosion constant $K_{p,l}$, and critical erosion shear stress $\tau_{e,l}$. Erosion follows a Partheniades-type excess-shear formulation. Erosion is disabled if the local water depth is below $h_{\mathrm{ero,min}} = \max(0.1\ \mathrm{m},\ 10 h_{\mathrm{tiny}})$, where h_{tiny} is the RDycore wet-dry threshold. If $h < h_{\mathrm{ero,min}}$, no sediment is eroded from the bed. For an erodible layer l, the potential total erosion flux is

https://doi.org/10.5194/egusphere-2026-4859
Preprint. Discussion started: 20 August 2026

$$E_\ell^{\text{pot}} = \begin{cases} K_{p,\ell}\left(\frac{\tau_b - \tau_{e,\ell}}{\tau_{e,\ell}}\right), & \tau_b > \tau_{e,\ell}, \\ 0, & \tau_b \le \tau_{e,\ell}. \end{cases} \tag{A8}$$

The implementation erodes bed layers sequentially. It first attempts to erode the active layer. If the active layer is exhausted within the time step, the remaining erosion time is applied to the next substrate layer, and so on. For a time step Δt, the eroded mass from layer l is limited by available bed mass:

$$\Delta M_\ell^{\text{ero}} = \min\left(M_\ell, E_\ell^{\text{pot}} \Delta t_\ell\right), \tag{A9}$$

where Δt_ℓ is the portion of the time step during which layer l is exposed. The eroded mass is partitioned among classes in proportion to the layer composition:

$$\Delta M_{\ell,s}^{\text{ero}} = \Delta M_\ell^{\text{ero}} \frac{M_{\ell,s}}{M_\ell}. \tag{A10}$$

The class-specific erosion flux entering the water-column sediment equation is then

$$E_s = \frac{1}{\Delta t} \sum_\ell \Delta M_{\ell,s}^{\text{ero}}. \tag{A11}$$

Deposition is computed independently for each sediment class. If $\tau_{d,s} > 0$ and $\tau_b < \tau_{d,s}$, the deposition flux is

$$D_s = w_s c_s \left(1 - \frac{\tau_b}{\tau_{d,s}}\right). \tag{A12}$$

Otherwise, $D_s = 0$.

Thus deposition is disabled by setting $\tau_{d,s} = 0$, as in the passive sediment-transport tests. The deposited mass added to the active bed layer is

$$\Delta M_{a,s}^{\text{dep}} = \max[0, (E_s - F_s^{\text{net}})\Delta t]. \tag{A13}$$

The model also stores F_s^{net} as a diagnostic field for each sediment class.

A3 Active-layer update

After erosion and deposition are applied, RDycore-sediment updates the active layer in each cell. The layer thickness implied by the current mass is computed from

$$H_\ell = \frac{M_\ell}{\bar{\rho}_\ell (1 - \phi_\ell)}, \tag{A14}$$

where the current composition-weighted grain density is

$$\bar{\rho}_\ell = \sum_{s=1}^{N_s} \left(\frac{M_{\ell,s}}{M_\ell}\right) \rho_s. \tag{A15}$$

If the active layer is thicker than the prescribed active-layer thickness H_a, a proportional amount of active-layer mass is transferred downward to the first substrate layer. If the active layer is thinner than H_a, mass is drawn upward from the substrate layers until the active layer is refilled or the substrate mass is exhausted. This operation conserves class-specific bed mass locally, but it does not change the computational bed elevation.

The active-layer concentration used for erosion-property interpolation is updated by mixing with the donor layer concentration when substrate material is moved into the active layer:

https://doi.org/10.5194/egusphere-2026-4859
Preprint. Discussion started: 20 August 2026

$$C_a^{\text{new}} = \frac{C_a M_a + C_{\text{donor}} \Delta M}{M_a + \Delta M}. \quad \text{(A16)}$$

A4 Roe water flux and upwind sediment flux

At each edge, RDycore first computes the shallow-water Roe flux using only the hydrodynamic states h, u, and v. Let the unit normal direction be represented by $\boldsymbol{n} = (n_x, n_y)$, and define the normal velocity

$$u_n = u n_x + v n_y. \quad \text{(A17)}$$

The physical water fluxes on the left and right sides are

$$F_{h,L} = h_L u_{n,L}, \quad \text{(A18)}$$

$$F_{h,R} = h_R u_{n,R}. \quad \text{(A19)}$$

The Roe numerical water flux is

$$\hat{F}_h^{\text{Roe}} = \frac{1}{2}\left(F_{h,L} + F_{h,R}\right) - \frac{1}{2}\left[\mathbf{R}_{\text{SWE}} |\boldsymbol{\Lambda}_{\text{SWE}}| \Delta \mathbf{W}_{\text{SWE}}\right]_h. \quad \text{(A20)}$$

This flux determines the sediment donor concentration in the upwind formula given in Sect. 2.3. The coupling is one-way: the Roe eigenvalues, Roe averages, water flux, and momentum fluxes are computed from the shallow-water variables only. Sediment concentrations are used only after the hydrodynamic mass flux has been obtained. In wet cells, concentration is recovered as

$$c_s = \frac{m_s}{h}. \quad \text{(A21)}$$

For dry or nearly dry cells, the code sets velocity and concentration to zero when $h < h_{\text{tiny}}$. Velocities are regularized using the ANUGA-style form (Mungkasi & Roberts, 2012)

$$u = \frac{(hu)h}{h^2 + h_\epsilon^2}, \quad \text{(A22)}$$

$$v = \frac{(hv)h}{h^2 + h_\epsilon^2}. \quad \text{(A23)}$$

where h_ϵ is the regularization depth.

A5 Hydrostatic reconstruction

For simulations using hydrostatic reconstruction, RDycore-sediment reconstructs water depth at each internal edge before computing the Roe flux. For left and right bed elevations z_L and z_R,

$$z^* = \max(z_L, z_R), \quad \text{(A24)}$$

$$h_L^* = \max[0,\ h_L + z_L - z^*], \quad \text{(A25)}$$

$$h_R^* = \max[0,\ h_R + z_R - z^*]. \quad \text{(A26)}$$

The sediment concentration is preserved during reconstruction:

$$c_{s,L}^* = c_{s,L}, \quad \text{(A27)}$$

$$c_{s,R}^* = c_{s,R}, \quad \text{(A28)}$$

https://doi.org/10.5194/egusphere-2026-4859
Preprint. Discussion started: 20 August 2026

and the reconstructed conservative sediment variables are

$$m_{s,L}^{*} = h_L^{*} c_{s,L}, \tag{A29}$$

$$m_{s,R}^{*} = h_R^{*} c_{s,R}. \tag{A30}$$

The same Roe water flux and upwind sediment flux are then evaluated using the reconstructed depths. Hydrostatic pressure corrections are applied only to the momentum equations. They do not add any additional sediment source term.

A6 Boundary conditions and external sediment sources

For reflecting boundaries, RDycore-sediment reflects the hydrodynamic velocity and copies the interior sediment concentration to the exterior Riemann state:

$$c_{s,R} = c_{s,L}. \tag{A31}$$

For Dirichlet boundaries, the prescribed boundary sediment value is used to define the exterior sediment state. The boundary sediment flux again uses the sign of the hydrodynamic Roe mass flux:

$$\hat{F}_{m_s}^{\partial\Omega} = \hat{F}_h^{\partial\Omega} c_s^{\mathrm{up}}. \tag{A32}$$

External sediment sources (e.g., hillslope soil erosion) enter the m_s equation as S_{m_s}. In the implementation, these sources are tapered in shallow water with

$$S_{m_s}^{\mathrm{eff}} = S_{m_s} \min\left(1, \frac{h}{h_{\mathrm{src,min}}}\right), \tag{A33}$$

where $h_{\mathrm{src,min}}$ is a minimum water depth that prevents large sediment additions in nearly dry cells.

A7 Boundary flux

RDycore-sediment is able to output boundary fluxes of water and sediment as diagnostic variables. At each boundary edge e, the Roe solver calculates the outward-normal numerical water flux $F_{h,e}$. The corresponding sediment flux per unit edge length is

$$F_{s,e} = F_{h,e} c_{s,e}^{up}, \tag{A34}$$

where $c_{s,e}^{up}$ is the edge's upwind concentration (Eq. 12). The sediment mass discharge across the complete boundary is

$$Q_s(t) = \sum_{e \in \Gamma} L_e F_{h,e}(t) c_{s,e}^{\mathrm{up}}(t), \tag{A35}$$

where L_e is the boundary-edge length. Positive values represent sediment export from the computational domain, while negative values represent sediment import. RDycore accumulates the flux during every forward-Euler time step. The value written for output interval ΔT is the time-averaged discharge:

$$\overline{Q_s} = \frac{1}{\Delta T} \sum_t \Delta t\, Q_s(t). \tag{A36}$$

https://doi.org/10.5194/egusphere-2026-4859
Preprint. Discussion started: 20 August 2026

Appendix B Sediment MMS Equations

The sediment transport equation with bed exchange and an MMS source term is written as

$$\frac{\partial(hc_s)}{\partial t}+\frac{\partial(huc_s)}{\partial x}+\frac{\partial(hvc_s)}{\partial y}=F_s^{\mathrm{net}}+S_{m_s}^{\mathrm{MMS}}, \quad \text{(B1)}$$

where u and v are depth-averaged velocities, $F_s^{\mathrm{net}}=E_s-D_s$ is the net erosion-deposition flux, and $S_{m_s}^{\mathrm{MMS}}$ is the manufactured source term.

The manufactured sediment concentrations are

$$c_0(x,y,t)=C[1+\sin(Kx)\sin(Ky)]\exp\left(\frac{t}{T}\right), \quad \text{(B2)}$$

$$c_1(x,y,t)=C[1+\sin(Kx)\sin(Ky)]\exp\left(-\frac{t}{T}\right), \quad \text{(B3)}$$

$$c_2(x,y,t)=C[1+\sin(Kx)\sin(Ky)]\exp\left(-\frac{t}{T}\right), \quad \text{(B4)}$$

where $K=\pi/L$, $L=5$ m, $T=20$ s, and the prescribed concentration scale $C=0.5$.

For a compact class-wise form, define $\alpha_0=1$ and $\alpha_1=\alpha_2=-1$. Then

$$c_s(x,y,t)=C[1+\sin(Kx)\sin(Ky)]\exp\left(\alpha_s\frac{t}{T}\right). \quad \text{(B5)}$$

The derivatives used to construct the MMS sediment source are

$$\frac{\partial c_s}{\partial x}=CK\cos(Kx)\sin(Ky)\exp\left(\alpha_s\frac{t}{T}\right), \quad \text{(B6)}$$

$$\frac{\partial c_s}{\partial y}=CK\sin(Kx)\cos(Ky)\exp\left(\alpha_s\frac{t}{T}\right), \quad \text{(B7)}$$

$$\frac{\partial c_s}{\partial t}=\frac{\alpha_s}{T}c_s. \quad \text{(B8)}$$

Substituting the manufactured solution into the conservative sediment equation gives

$$S_{m_s}^{\mathrm{MMS}}=\frac{\partial(hc_s)}{\partial t}+\frac{\partial(huc_s)}{\partial x}+\frac{\partial(hvc_s)}{\partial y}-F_s^{\mathrm{net}}. \quad \text{(B9)}$$

Expanding the derivatives,

$$S_{m_s}^{\mathrm{MMS}}=c_s\frac{\partial h}{\partial t}+h\frac{\partial c_s}{\partial t}+uc_s\frac{\partial h}{\partial x}+hc_s\frac{\partial u}{\partial x}+hu\frac{\partial c_s}{\partial x}+vc_s\frac{\partial h}{\partial y}+hc_s\frac{\partial v}{\partial y}+hv\frac{\partial c_s}{\partial y}-F_s^{\mathrm{net}}. \quad \text{(B10)}$$

In RDycore-sediment, the net bed flux F_s^{net} is evaluated using the same erosion and deposition routines used in the prognostic sediment simulations. Therefore, the MMS source term verifies the sediment advection operator together with the implementation of the erosion-deposition coupling.

Numerical accuracy is quantified using the cell-area-weighted L_1, L_2, and L_∞ error norms evaluated for each hydrodynamic and sediment solution variable. The convergence rates are estimated by linear regression of the logarithmic error against the logarithm of the total number of cells, following the RDycore MMS procedure. Let $U_{i,k}^{\mathrm{num}}$ and $U_{i,k}^{\mathrm{MMS}}$ denote the numerical and manufactured values, respectively, of solution component k in cell i, where k represents h, hu, hv, or $m_s=hc_s$. The cellwise error is

$$e_{i,k}=U_{i,k}^{\mathrm{num}}-U_{i,k}^{\mathrm{MMS}}. \quad \text{(B11)}$$

https://doi.org/10.5194/egusphere-2026-4859
Preprint. Discussion started: 20 August 2026

Thus, the three norms are

$$L_{1,k} = \sum_{i=1}^{N_c} A_i \left|e_{i,k}\right|, \tag{B12}$$

$$L_{2,k} = \left(\sum_{i=1}^{N_c} A_i \, e_{i,k}^2\right)^{1/2}, \tag{B13}$$

$$L_{\infty,k} = \max_{1 \le i \le N_c} \left|e_{i,k}\right|, \tag{B14}$$

where A_i is cell area, N_c is the number of cells.

Code and data availability

The exact RDycore-sediment source code used in this study is archived on Zenodo at https://doi.org/10.5281/zenodo.21894232 (Feng, 2026a). The processed input data, model outputs, comparison data, postprocessing and plotting scripts used to reproduce the figures and tables are archived on Zenodo at https://doi.org/10.5281/zenodo.21894710 (Feng, 2026b). The production Houston Harvey simulations were run on the DOE-supported Perlmutter system at NERSC. Full reruns on other machines may require additional large input files and machine-specific build/run configuration.

Author contributions

DF, ZT, GB, and DX designed the methodology and numerical experiments. DF, GB, and JJ developed the software. DF performed the analysis and visualization of the results. DF wrote the initial draft of the manuscript. All authors contributed to the discussion and interpretation of the results and to the review and editing of the manuscript.

Competing interests

At least one of the (co-)authors is a member of the editorial board of Geoscientific Model Development.

Disclaimer

Copernicus Publications remains neutral with regard to jurisdictional claims made in the text, published maps, institutional affiliations, or any other geographical representation in this paper. While Copernicus Publications makes every effort to include appropriate place names, the final responsibility lies with the authors. Views expressed in the text are those of the authors and do not necessarily reflect the views of the publisher.

https://doi.org/10.5194/egusphere-2026-4859
Preprint. Discussion started: 20 August 2026

Acknowledgements

All model simulations were performed using resources available through the National Energy Research Scientific Computing Center (NERSC), a US Department of Energy Office of Science User Facility located at Lawrence Berkeley National Laboratory, operated under contract no. DEAC02-05CH11231 using NERSC award BER-ERCAP0036829. The Pacific Northwest National Laboratory (PNNL) is operated for DOE by Battelle Memorial Institute, United States, under contract DE-AC05-76RL01830.

Financial support

This research was supported through the U.S. Department of Energy Office of Science's Scientific Discovery through Advanced Computing (SciDAC) program, the Advanced Scientific Computing Research (ASCR) program, and the Biological and Environmental Research's (BER's) Earth System Model Development program area via the SciDAC project "Capturing the Dynamics of Compound Flooding in E3SM".

References

Audusse, E., & Bristeau, M.-O. (2003). Transport of Pollutant in Shallow Water: A Two Time Steps Kinetic Method. *ESAIM: Mathematical Modelling and Numerical Analysis*, *37*(2), 389-416. https://doi.org/10.1051/m2an:2003034

Balay, S., Abhyankar, S., Adams, M., Benson, S., Brown, J., Brune, P., Buschelman, K., Constantinescu, E., Dalin, L., & Dener, A. (2021). *PETSc/TAO users manual, argonne national laboratory*.

Berhe, A. A., Barnes, R. T., Six, J., & Marín-Spiotta, E. (2018). Role of soil erosion in biogeochemical cycling of essential elements: carbon, nitrogen, and phosphorus. *Annual Review of Earth and Planetary Sciences*, *46*(1), 521-548. https://doi.org/10.1146/annurev-earth-082517-010018

Bisht, G., Xu, D., Johnson, J., Brown, J., Knepley, M., Adams, M., Feng, D., Hao, D., Engwirda, D., & Kumar, M. (2025). Development of a River Dynamical Core for E3SM to simulate compound flooding on Exascale-class heterogeneous supercomputers. *Environmental Modelling & Software*, 106804. https://doi.org/10.1016/j.envsoft.2025.106804

Brown, J., Abdelfattah, A., Barra, V., Beams, N., Camier, J.-S., Dobrev, V., Dudouit, Y., Ghaffari, L., Kolev, T., & Medina, D. (2021). libCEED: Fast algebra for high-order element-based discretizations. *Journal of Open Source Software*, *6*(63), 2945. https://doi.org/10.21105/joss.02945

Brunner, G. W., & Gibson, S. (2005). Sediment transport modeling in HEC RAS. In *Impacts of global climate change* (pp. 1-12). https://doi.org/10.1061/40792(173)442

Cohen, S., Kettner, A. J., Syvitski, J. P., & Fekete, B. M. (2013). WBMsed, a distributed global-scale riverine sediment flux model: Model description and validation. *Computers & Geosciences*, *53*, 80-93. https://doi.org/10.1016/j.cageo.2011.08.011

https://doi.org/10.5194/egusphere-2026-4859
Preprint. Discussion started: 20 August 2026

Dethier, E. N., Renshaw, C. E., & Magilligan, F. J. (2022). Rapid changes to global river suspended sediment flux by humans. *Science*, *376*(6600), 1447-1452. https://doi.org/10.1126/science.abn7980

Feng, D., Tan, Z., Engwirda, D., Liao, C., Xu, D., Bisht, G., Zhou, T., Li, H.-Y., & Leung, R. (2022). Investigating coastal backwater effects and flooding in the coastal zone using a global river transport model on an unstructured mesh. *Hydrology and Earth System Sciences*, *26*(21), 5473-5491. https://doi.org/10.5194/hess-26-5473-2022

Feng, D., Tan, Z., Engwirda, D., Wolfe, J. D., Xu, D., Liao, C., Bisht, G., Benedict, J. J., Zhou, T., & Li, H. Y. (2024). Simulation of compound flooding using river-ocean two-way coupled E3SM ensemble on variable-resolution meshes. *Journal of Advances in Modeling Earth Systems*, *16*(6), e2023MS004054. https://doi.org/10.1029/2023MS004054

Feng, D., Tan, Z., Pinel, S., Xu, D., Amaral, J. H. F., Fassoni-Andrade, A. C., Bonnet, M.-P., & Bisht, G. (2025). Drivers and impacts of sediment deposition in Amazonian floodplains. *Nature Communications*, *16*(1), 3148. https://doi.org/10.1038/s41467-025-57495-1

Feng, D. (2026a). *RDycore-sediment* [Computer software]. Zenodo. https://doi.org/10.5281/zenodo.21894232

Feng, D. (2026b). *Data and scripts for the RDycore-sediment manuscript* [Dataset]. Zenodo. https://doi.org/10.5281/zenodo.21894710

Feng, D., Tan, Z., Xu, D., Li, L., & Bisht, G. (2026). An integrated modeling framework for sediment dynamics during urban flooding: Application to Hurricane Harvey in Houston. *Water Resources Research*, *62*(5), e2025WR042040. https://doi.org/10.1029/2025WR042040

Golaz, J. C., Caldwell, P. M., Van Roekel, L. P., Petersen, M. R., Tang, Q., Wolfe, J. D., Abeshu, G., Anantharaj, V., Asay-Davis, X. S., & Bader, D. C. (2019). The DOE E3SM coupled model version 1: Overview and evaluation at standard resolution. *Journal of Advances in Modeling Earth Systems*, *11*(7), 2089-2129. https://doi.org/10.1029/2018MS001603

Golaz, J. C., Van Roekel, L. P., Zheng, X., Roberts, A. F., Wolfe, J. D., Lin, W., Bradley, A. M., Tang, Q., Maltrud, M. E., & Forsyth, R. M. (2022). The DOE E3SM model version 2: Overview of the physical model and initial model evaluation. *Journal of Advances in Modeling Earth Systems*, *14*(12), e2022MS003156. https://doi.org/10.1029/2022MS003156

Gorgoglione, A., Bombardelli, F. A., Pitton, B. J., Oki, L. R., Haver, D. L., & Young, T. M. (2019). Uncertainty in the parameterization of sediment build-up and wash-off processes in the simulation of sediment transport in urban areas. *Environmental Modelling & Software*, *111*, 170-181. https://doi.org/10.1016/j.envsoft.2018.09.022

Guan, Q., Feng, L., Tang, J., Park, E., Ali, T. A., & Zheng, Y. (2022). Trends in river total suspended sediments driven by dams and soil erosion: A comparison between the Yangtze and Mekong rivers. *Water Resources Research*, *58*(10), e2022WR031979. https://doi.org/10.1029/2022WR031979

Heng, B., Sander, G. C., Armstrong, A., Quinton, J., Chandler, J. H., & Scott, C. F. (2011). Modeling the dynamics of soil erosion and size-selective sediment transport over nonuniform topography in flume-scale experiments. *Water Resources Research*, *47*(2). https://doi.org/10.1029/2010WR009375

Jomaa, S., Barry, D. A., Heng, B., Brovelli, A., Sander, G., & Parlange, J. Y. (2012). Influence of rock fragment coverage on soil erosion and hydrological response: Laboratory flume experiments and modeling. *Water Resources Research*, *48*(5). https://doi.org/10.1029/2011WR011255

Kettner, A. J., & Syvitski, J. P. (2008). HydroTrend v. 3.0: A climate-driven hydrological transport model that simulates discharge and sediment load leaving a river system. *Computers & Geosciences*, *34*(10), 1170-1183. https://doi.org/10.1016/j.cageo.2008.02.008

Kim, J., Ivanov, V. Y., & Katopodes, N. D. (2013). Modeling erosion and sedimentation coupled with hydrological and overland flow processes at the watershed scale. *Water Resources Research*, *49*(9), 5134-5154. https://doi.org/10.1002/wrcr.20373

Lamb, M. P., de Leeuw, J., Fischer, W. W., Moodie, A. J., Venditti, J. G., Nittrouer, J. A., Haught, D., & Parker, G. (2020). Mud in rivers transported as flocculated and suspended bed material. *Nature Geoscience*, *13*(8), 566-570. https://doi.org/10.1038/s41561-020-0602-5

Le, M. H., Cordier, S., Lucas, C., & Cerdan, O. (2015). A faster numerical scheme for a coupled system modeling soil erosion and sediment transport. *Water Resources Research*, *51*(2), 987-1005. https://doi.org/10.1002/2014WR015690

Lesser, G. R., Roelvink, J. v., van Kester, J. T. M., & Stelling, G. (2004). Development and validation of a three-dimensional morphological model. *Coastal Engineering*, *51*(8-9), 883-915. https://doi.org/10.1016/j.coastaleng.2004.07.014

Li, H., Wigmosta, M. S., Wu, H., Huang, M., Ke, Y., Coleman, A. M., & Leung, L. R. (2013). A physically based runoff routing model for land surface and earth system models. *Journal of Hydrometeorology*, *14*(3), 808-828. https://doi.org/10.1175/JHM-D-12-015.1

Li, H.-Y., Tan, Z., Ma, H., Zhu, Z., Abeshu, G., Zhu, S., Cohen, S., Zhou, T., Xu, D., & Leung, L.-Y. R. (2022). A new large-scale suspended sediment model and its application over the United States. *Hydrology and Earth System Sciences*, *26*(3), 665–688. https://doi.org/10.5194/hess-26-665-2022

Li, S., & Duffy, C. J. (2011). Fully coupled approach to modeling shallow water flow, sediment transport, and bed evolution in rivers. *Water Resources Research*, *47*(3). https://doi.org/10.1029/2010WR009751

Liu, M., Raymond, P. A., Lauerwald, R., Zhang, Q., Trapp-Müller, G., Davis, K. L., Moosdorf, N., Xiao, C., Middelburg, J. J., & Bouwman, A. F. (2024). Global riverine land-to-ocean carbon export constrained by observations and multi-model assessment. *Nature Geoscience*, *17*(9), 896-904. https://doi.org/10.1038/s41561-024-01524-z

Mungkasi, S., & Roberts, S. (2012). ANUGA software for numerical simulations of shallow water flow. *Journal of Computer Science and Information*, 5(1), 8 pp. https://doi.org/10.21609/jiki.v5i1.180

Partheniades, E. (1965). Erosion and deposition of cohesive soils. *Journal of the Hydraulics Division*, *91*(1), 105-139. https://doi.org/10.1061/JYCEAJ.0001165

Peng, D., Tan, Z., Yuan, T., Wu, P., Song, Z., Zhang, P., Huang, S., Zhang, Y., Lei, T., & Middleton, B. A. (2025). Human perturbations to mercury in global rivers. *Science Advances*, *11*(24), eadw0471. https://doi.org/10.1126/sciadv.adw0471

https://doi.org/10.5194/egusphere-2026-4859
Preprint. Discussion started: 20 August 2026

Regnier, P., Resplandy, L., Najjar, R. G., & Ciais, P. (2022). The land-to-ocean loops of the global carbon cycle. *Nature*, *603*(7901), 401-410. https://doi.org/10.1038/s41586-021-04339-9

Sarkhosh, P. (2021). *Stoker solution package*. In (Version 1.0.0) Zenodo. https://doi.org/10.5281/zenodo.5598374

Shimizu, Y., Nelson, J., Arnez Ferrel, K., Asahi, K., Giri, S., Inoue, T., Iwasaki, T., Jang, C. L., Kang, T., & Kimura, I. (2020). Advances in computational morphodynamics using the International River Interface Cooperative (iRIC) software. *Earth Surface Processes and Landforms*, *45*(1), 11-37. https://doi.org/10.1002/esp.4653

Steinberg, S., & Roache, P. J. (1985). Symbolic manipulation and computational fluid dynamics. *Journal of Computational Physics*, *57*(2), 251-284. https://doi.org/10.1016/0021-9991(85)90045-2

Stoker, J. J. (2019). *Water waves: The mathematical theory with applications*. Courier Dover Publications.

Sun, J., Zhang, F., Zhang, X., Lin, B., Yang, Z., Yuan, B., & Falconer, R. A. (2021). Severely declining suspended sediment concentration in the heavily dammed Changjiang fluvial system. *Water Resources Research*, *57*(11), e2021WR030370. https://doi.org/10.1029/2021WR030370

Syvitski, J. P., & Milliman, J. D. (2007). Geology, geography, and humans battle for dominance over the delivery of fluvial sediment to the coastal ocean. *The Journal of Geology*, *115*(1), 1-19. https://doi.org/10.1086/509246

Syvitski, J. P., Vörösmarty, C. J., Kettner, A. J., & Green, P. (2005). Impact of humans on the flux of terrestrial sediment to the global coastal ocean. *Science*, *308*(5720), 376-380. https://doi.org/10.1126/science.1109454

Tan, Z., Leung, L. R., Li, H.-Y., Tesfa, T., Zhu, Q., Yang, X., Liu, Y., & Huang, M. (2021). Increased extreme rains intensify erosional nitrogen and phosphorus fluxes to the northern Gulf of Mexico in recent decades. *Environmental Research Letters*, *16*(5), 054080. https://doi.org/10.1088/1748-9326/abf006

Tan, Z., Leung, L. R., Li, H. Y., & Cohen, S. (2022). Representing global soil erosion and sediment flux in Earth System Models. *Journal of Advances in Modeling Earth Systems*, *14*(1), e2021MS002756. https://doi.org/10.1029/2021MS002756

Tan, Z., Leung, L. R., Li, H. Y., & Tesfa, T. (2018). Modeling sediment yield in land surface and earth system models: Model comparison, development, and evaluation. *Journal of Advances in Modeling Earth Systems*, *10*(9), 2192-2213. https://doi.org/10.1029/2017MS001270

Tan, Z., Leung, L. R., Li, H. Y., Tesfa, T., Zhu, Q., & Huang, M. (2020). A substantial role of soil erosion in the land carbon sink and its future changes. *Global Change Biology*, *26*(4), 2642-2655. https://doi.org/10.1111/gcb.14982

Tangi, M., Bizzi, S., Fryirs, K., & Castelletti, A. (2022). A dynamic, network scale sediment (dis) connectivity model to reconstruct historical sediment transfer and river reach sediment budgets. *Water Resources Research*, *58*(2), e2021WR030784. https://doi.org/10.1029/2021WR030784

Tassi, P., Benson, T., Delinares, M., Fontaine, J., Huybrechts, N., Kopmann, R., Pavan, S., Pham, C.-T., Taccone, F., & Walther, R. (2023). GAIA-a unified framework for sediment transport and bed evolution in rivers, coastal seas and transitional waters in the TELEMAC-MASCARET modelling system. *Environmental Modelling & Software*, *159*, 105544. https://doi.org/10.1016/j.envsoft.2022.105544

https://doi.org/10.5194/egusphere-2026-4859
Preprint. Discussion started: 20 August 2026

Vanzo, D., Peter, S., Vonwiller, L., Bürgler, M., Weberndorfer, M., Siviglia, A., Conde, D., & Vetsch, D. F. (2021). BASEMENT v3: A modular freeware for river process modelling over multiple computational backends. *Environmental Modelling & Software*, *143*, 105102. https://doi.org/10.1016/j.envsoft.2021.105102

Villaret, C., Hervouet, J.-M., Kopmann, R., Merkel, U., & Davies, A. G. (2013). Morphodynamic modeling using the Telemac finite-element system. *Computers & Geosciences*, *53*, 105-113. https://doi.org/10.1016/j.cageo.2011.10.004

Vörösmarty, C. J., Meybeck, M., Fekete, B., Sharma, K., Green, P., & Syvitski, J. P. (2003). Anthropogenic sediment retention: major global impact from registered river impoundments. *Global and planetary change*, *39*(1-2), 169-190. https://doi.org/10.1016/S0921-8181(03)00023-7

Walling, D. E. (1983). The sediment delivery problem. *Journal of Hydrology*, *65*(1-3), 209-237. https://doi.org/10.1016/0022-1694(83)90217-2

Wang, S., Fu, B., Piao, S., Lü, Y., Ciais, P., Feng, X., & Wang, Y. (2016). Reduced sediment transport in the Yellow River due to anthropogenic changes. *Nature Geoscience*, *9*(1), 38-41. https://doi.org/10.1038/ngeo2602

Ward, N. D., Megonigal, J. P., Bond-Lamberty, B., Bailey, V. L., Butman, D., Canuel, E. A., Diefenderfer, H., Ganju, N. K., Goñi, M. A., & Graham, E. B. (2020). Representing the function and sensitivity of coastal interfaces in Earth system models. *Nature Communications*, *11*(1), 2458. https://doi.org/10.1038/s41467-020-16236-2

Wohl, E., Bledsoe, B. P., Jacobson, R. B., Poff, N. L., Rathburn, S. L., Walters, D. M., & Wilcox, A. C. (2015). The natural sediment regime in rivers: Broadening the foundation for ecosystem management. *BioScience*, *65*(4), 358-371. https://doi.org/10.1093/biosci/biv002

Xu, D., Bisht, G., Feng, D., Tan, Z., Hao, D., Engwirda, D., Benedict, J. J., Tran, V. N., Kumar, M., Ivanov, V., & Leung, L. R. (2026). Significant Rural Contributions to Severe Coastal Urban Flooding Through Flow Connectivity. *Geophysical Research Letters*, *53*(14), e2026GL122550. https://doi.org/10.1029/2026GL122550